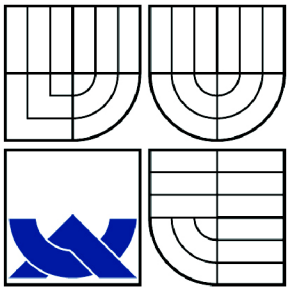

VYSOKÉ UČENÍ TECHNICKÉ V BRNĚ

BRNO UNIVERSITY OF TECHNOLOGY

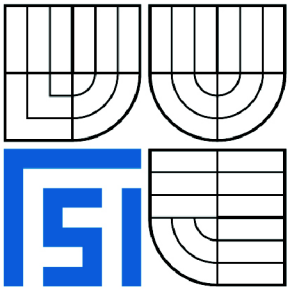

FAKULTA STROJNÍHO INŽENÝRSTVÍ
ÚSTAV MATEMATIKY

FACULTY OF MECHANICAL ENGINEERING
INSTITUTE OF MATHEMATICS

COMPUTATIONAL MODELLING OF A LABORATORY BURNER USING FLUENT CODE

VÝPOČTOVÉ MODELOVÁNÍ LABORATORNÍHO HOŘÁKU PROGRAMEM FLUENT

DIPLOMOVÁ PRÁCE
MASTER'S THESIS

AUTOR PRÁCE — Bc. JAKUB BROUKAL
AUTHOR

VEDOUCÍ PRÁCE — doc. Ing. JIŘÍ HÁJEK, Ph.D.
SUPERVISOR

BRNO 2009

Vysoké učení technické v Brně, Fakulta strojního inženýrství

Ústav matematiky
Akademický rok: 2008/2009

ZADÁNÍ DIPLOMOVÉ PRÁCE

student(ka): Bc. Jakub Broukal

který/která studuje v **magisterském navazujícím studijním programu**

obor: **Matematické inženýrství (3901T021)**

Ředitel ústavu Vám v souladu se zákonem č.111/1998 o vysokých školách a se Studijním a zkušebním řádem VUT v Brně určuje následující téma diplomové práce:

Výpočtové modelování laboratorního hořáku programem FLUENT

v anglickém jazyce:

Computational modelling of a laboratory burner using FLUENT code

Stručná charakteristika problematiky úkolu:

Bude proveena simulace jednoduchého laboratorního hořáku. Bude vyhodnocena použitelnost modelu turbulentního spalování, umožňující detailní popis kinetiky chemických reakcí. Pro srovnání bude použit jednoduchý model spalování podle Magnussena a Hjertagera.

Cíle diplomové práce:

- Seznámit se s problematikou turbulentního difúzního spalování
- Seznámit se s metodami numerických výpočtů turbulentního difúzního spalování v programu FLUENT
- Provést simulaci laboratorního hořáku
- Vyhodnotit výsledky

Seznam odborné literatury:

[1] FLUENT 6.2.16 User's Guide, Fluent, Inc., Lebanon, 2005
[2] Versteeg, H.K., and Malalasekera, W. "An introduction to computational fluid dynamics: The finite volume method", Longman Group Ltd., 1995
[3] Warnatz J., Maas U., and Dibble R.W. "Combustion", Springer-Verlag Berlin Heidelberg, 1996

Vedoucí diplomové práce: doc. Ing. Jiří Hájek, Ph.D.

Termín odevzdání diplomové práce je stanoven časovým plánem akademického roku 2008/2009.

V Brně, dne 19.11.2008

L.S.

prof. RNDr. Josef Šlapal, CSc. Ředitel ústavu	doc. RNDr. Miroslav Doupovec, CSc. Děkan fakulty

Abstract

This thesis focuses on comparing various turbulence and chemical models on an exemplar free methane jet issuing into air. First, a theoretical overview of the models is presented followed by CFD (Ansys Fluent) simulations of the flame using the chosen models. As a part of the thesis an experimental measurement is performed and evaluated. Finally, both spectrometric results and Fluent-predicted data are compared.

Abstrakt

Tato diplomová práce je zaměřena na porovnání různých turbulentních a chemických modelů na příkladu volné metanové trysky ústící do vzduchu. Nejprve je uveden teoretický úvod k modelům, následován CFD (Ansys Fluent) simulacemi plamene pomocí vybraných modelů. Jako součást práce je provedeno a vyhodnoceno experimentální měření. V závěru jsou experimentální výsledky porovnány s nasimulovanými daty.

Keywords

Methane-air combustion, free jet, turbulence models, chemical models, diffusion flame, reaction mechanism

Klíčová slova

Spalování metanu ve vzduchu, volná tryska, modely turbulence, chemické modely, difusní plamen, reakční mechanismy

BROUKAL, J. *Výpočtové modelování laboratorního hořáku programem FLUENT.* Brno: Vysoké učení technické v Brně, Fakulta strojního inženýrství, 2009. 61 s. Vedoucí diplomové práce doc. Ing. Jiří Hájek, Ph.D.

Declaration

I hereby declare that this thesis is a result of my own work under the supervision of doc. Ing. Jiří Hájek, Ph.D. All the used sources are listed in the bibliography.

Prohlášení

Prohlašuji, že jsem tuto diplomovou práci vypracoval samostatně pod vedením doc. Ing. Jiřího Hájka, Ph.D. Veškeré použité zdroje jsou uvedeny v seznamu literatury.

Acknowledgement

First and foremost I would like to thank my supervisor doc. Ing. Jiří Hájek, Ph.D. for introducing me into this up to now, from my point of view, unknown field of combustion. His wide knowledge and supportive approach have been of great value.
Next I would like to thank doc. RNDr. František Krčma, Ph.D. for helping us with the spectrometric experiment, prof. RNDr. Vladimír Aubrecht, CSc. and prof. Ing. Oldřich Zmeškal, CSc. for lending the high speed and thermal camera and also Ing. Vít Kermes, Ph.D. and Ing. Petr Bělohradský for their general help during experiments.
I would also thank my family for their huge support throughout my whole study.

Poděkování

Především bych chtěl poděkovat vedoucímu své diplomové práce doc. Ing. Jiřímu Hájkovi, Ph.D. za to, že mě uvedl do, pro mě do té doby neznámého, oboru spalování. Jeho obsáhlé vědomosti a podpora mi byla velkou oporou.
Dále bych chtěl poděkovat doc. RNDr. Františku Krčmovi, Ph.D. za pomoc při spektrometrickém měření, prof. RNDr. Vladimíru Aubrechtovi, CSc. a Ing. Oldřichu Zmeškalovi, CSc. za zapůjčení vysokorychlostní kamery a termokamery, a také Ing. Vítu Kermesovi, Ph.D. a Ing. Petru Bělohradskému za jejich všeobecnou pomoc při experimentech.
Rád bych poděkoval také své rodině za jejich velikou podporu během celého studia.

Table of contents

1 Introduction

1.1 Motivation

Combustion is a very important part of engineering. It has many applications and has been widely studied. With the upswing of computer computation, modelling and simulation large part of the combustion research focused on how to predict and examine different types of flames and how to convert theoretical findings into numerical models. These models are constantly analyzed, tested, improved and compared with experimental results.

In combustion processes, fuel and oxidizer (typically air) are mixed together and burned. It is very useful to distinguish from several combustion categories based upon whether the fuel and oxidizer is mixed first and burned later (*premixed combustion*) or whether mixing and burning occurs simultaneously (*nonpremixed combustion*). Each of these categories can be further divided based on whether the fluid flow is laminar or turbulent. Turbulent non-premixed (diffusion) flames are favoured in a majority of so-called power burners that are used especially in fired heaters and furnaces in chemical, petrochemical, and other processing industries. One of the reasons is that nonpremixed flames are safer to work with, since there is no risk of flashback. Turbulence is welcome because it enhances the mixing of fuel and oxidizer which often leads to a shorter flame. A special simple case of diffusion flames occurring in most power burners is the flame of a single free jet of gaseous fuel, issuing into an oxidizing atmosphere. Such simple flame when studied separately is called a "free jet flame" and it operates either in stagnant atmosphere or in a controlled co-flow.

In engineering it is important to know how things work and how can we predict them. In the field of combustion we are nowadays more or less capable of predicting the temperature, velocity, fluxes, species concentration and many other aspects of flames. But when we want to compare the predictions with experiments, it is very difficult or even impossible, as in the case of design supporting computations. And of course, industrial experts are often interested in the shape (height, width) of the visible flame, the visualisation of which is presently beyond our capabilities. Therefore the department of Process and Environmental Engineering is starting research on the topic of realistic predictive flame visualization and for this purpose it is required to validate sufficiently detailed, flow and chemistry models that could be subsequently coupled with a spectral radiation model.

1.2 Problem description

The problem considered in the thesis can be formulated as follows. A methane stream of small diameter discharges into quiescent air, where combustion occurs. The thin methane stream is generated using a nozzle of cylindrical shape. This simple set-up is to be investigated using numerical modelling and also experimentally.

1.3 Thesis overview

The primary goal of this diploma thesis is to compare the performance of basic turbulence and chemistry models applied to the considered flame.

In chapter 2 an overview of turbulent nonpremixed combustion theory is presented. In sections 2.1, 2.2 and 2.3 are introduced governing equations of turbulent and reacting flows along with a brief overview of various turbulence and chemical models. A brief overview of numerical approaches can be found in section 2.4. Review of recent research in the area of jet flame combustion is presented in chapter 3.

Chapter 4 deals with the experimental part of the study, the experiment settings and results, while chapter 5 treats the simulation performed in software system FLUENT. Sections 5.1 to 5.6 provide information about the models used in the work and details of the computations, while results are presented in section 5.7.

In chapter 6 are discussed and compared both the experimental and simulation results.

2 Theory

2.1 Governing equations of flow

Everything in our world, even fluids, is made of small particles. In the Ancient Greece they thought of them as atoms, we think of them as quarks and our successor might think of them as something else. But every time we can say that the world is discrete. On the other hand, if we look at things from a macroscopic point of view, many things seem continuous. Fortunately, when considering macroscopic scales, fluids even act continuously. Therefore, if we confine ourselves to macroscopic scales, we can make the assumption of continuity. And we also transpose the assumption of continuity to infinitesimal volumes.

The fundamental principles of the fluid dynamics are the conservation laws – conservation of mass, conservation of momentum (Newton's 2nd law of motion) and conservation of energy (1st law of thermodynamics). The form of these conservation laws varies depending on the approach we choose. Generally there are four approaches available, as shown in Tab 2-1. These approaches are practically equivalent (conservation equations derived using various approaches can be converted one in another); their difference lays in mathematic robustness and numerical solvability.

Tab 2-1 *Types of control volumes (Hájek 2007)*

	Size of control volume	Mobility of control volume
Approach A	Finite	non moveable
Approach B	Finite	moveable
Approach C	Infinitesimal	non moveable
Approach D	Infinitesimal	moveable

The difference between finite and infinitesimal control volumes is clear. The finite control volumes lead to *integral* equations while the infinitesimal control volumes lead to *partial differential* equations. Besides the size of the control volumes, the other property is their mobility. The non moveable control volume has its boundary fixed and the fluid flows through. Instead, the moveable control volume is dragged by the fluid and deformed in such a way, that it always contains the same fluid particles. In other words, the boundary is impenetrable and perfectly elastic. Equations derived using the non moveable control volumes are called *conservative* whereas equations derived using the moveable control volumes are called *non-conservative*. Based on historical developments, alternative names of conservative and non-conservative approaches are Euler- and Lagrange-approach, respectively (Hájek 2007).

Usually, transport equations are written according to approach C in Tab 2-1 (infinitesimal non moveable control volume) but when it comes to numerical solution, most of the computational software works with equations in integral (and

conservative) form. The reason is that the integration operator does not tie down the function characteristics of unknowns as much as the differentiation operator.

Navier-Stokes equation

Navier-Stokes equations are the basic governing partial-differential equations for a viscous, heat conducting fluid flow. Usually, the term Navier-Stokes equations refers to the following three equations – namely continuity equation (2.1) , momentum equation (2.2) and energy equation (2.3).

$$\frac{\partial \rho}{\partial t} + \nabla \cdot (\rho \mathbf{v}) = 0 \tag{2.1}$$

$$\begin{aligned}
\frac{\partial(\rho u)}{\partial t} + \nabla \cdot (\rho u \mathbf{v}) &= -\frac{\partial p}{\partial x} + \frac{\partial \tau_{xx}}{\partial x} + \frac{\partial \tau_{yx}}{\partial y} + \frac{\partial \tau_{zx}}{\partial z} + \rho f_x \\
\frac{\partial(\rho v)}{\partial t} + \nabla \cdot (\rho v \mathbf{v}) &= -\frac{\partial p}{\partial y} + \frac{\partial \tau_{xy}}{\partial x} + \frac{\partial \tau_{yy}}{\partial y} + \frac{\partial \tau_{zy}}{\partial z} + \rho f_y \\
\frac{\partial(\rho w)}{\partial t} + \nabla \cdot (\rho w \mathbf{v}) &= -\frac{\partial p}{\partial z} + \frac{\partial \tau_{xz}}{\partial x} + \frac{\partial \tau_{yz}}{\partial y} + \frac{\partial \tau_{zz}}{\partial z} + \rho f_z
\end{aligned} \tag{2.2}$$

$$\begin{aligned}
\frac{\partial(\rho e)}{\partial t} + \nabla \cdot (\rho e \mathbf{v}) = \rho q_v + \nabla \cdot (k \nabla T) - p \nabla v + \tau_{xx} \frac{\partial u}{\partial x} + \tau_{yx} \frac{\partial u}{\partial y} + \tau_{zx} \frac{\partial u}{\partial z} + \\
+ \tau_{xy} \frac{\partial v}{\partial x} + \tau_{yy} \frac{\partial v}{\partial y} + \tau_{zy} \frac{\partial v}{\partial z} + \tau_{xz} \frac{\partial w}{\partial x} + \tau_{yz} \frac{\partial w}{\partial y} + \tau_{zz} \frac{\partial w}{\partial z},
\end{aligned} \tag{2.3}$$

where the velocity $\mathbf{v} = (u, v, w)$ and $\mathbf{f} = (f_x, f_y, f_z)$ are volume forces.

In this set of equations we have 7 unknowns: ρ, u, v, w, p, e, T. In addition we have 9 stress components τ_{ij}, $i, j = x, y, z$. These stresses are caused by the fluid viscosity. Most fluids which are encountered in combustion problems can be considered as isotropic fluids. Thanks to this property only six of nine stresses are independent, as

$$\tau_{xy} = \tau_{yx}, \quad \tau_{xz} = \tau_{zx}, \quad \tau_{yz} = \tau_{zy}. \tag{2.4}$$

In 1845 G.G. Stokes proposed equations that relate the stresses to deformation speed (in the case of Newtonian fluids):

$$\begin{aligned}
\tau_{xx} &= \lambda \nabla \cdot \mathbf{v} + 2\mu \frac{\partial u}{\partial x}, \quad \tau_{yy} = \lambda \nabla \cdot \mathbf{v} + 2\mu \frac{\partial v}{\partial y}, \quad \tau_{zz} = \lambda \nabla \cdot \mathbf{v} + 2\mu \frac{\partial w}{\partial z} \\
\tau_{xy} &= \mu \left(\frac{\partial v}{\partial x} + \frac{\partial u}{\partial y} \right), \quad \tau_{xz} = \mu \left(\frac{\partial w}{\partial x} + \frac{\partial u}{\partial z} \right), \quad \tau_{yz} = \mu \left(\frac{\partial v}{\partial z} + \frac{\partial w}{\partial y} \right).
\end{aligned} \tag{2.5}$$

G.G Stokes also made a simplifying hypothesis about the relation between the second viscosity coefficient λ and the dynamic viscosity μ:

$$\lambda = -\frac{2}{3}\mu. \tag{2.6}$$

This relation has proven to be sufficiently accurate for most viscous flow problems.

At this point we can say that the nine stress components do not introduce any new unknown and since we have 7 unknowns and only 5 equations, to get a unique solution to the flow problem we need two more equations.

We can make use of the ideal-gas state equation

$$p = \frac{\rho R T}{M_s}, \tag{2.7}$$

where usually $R = 8,3143\ J.mol^{-1}.K^{-1}$.

Finally, the last needed equation can be for instance the relation between energy, temperature and pressure given by

$$e = e(p,T). \tag{2.8}$$

In particular cases (especially in incompressible fluids) the equation simply becomes $e = c_V T$.

Now that we have the same number of equations unknowns we can proceed to their solution. However, since 1845, when these equations have been proposed, there have been disputes about existence and uniqueness of the solution. In 1933 Jean Leray managed to prove existence and uniqueness, but only for 2-D problems. The problem of global existence and uniqueness in 3-D (for high Reynolds numbers) has not yet been solved. The Clay Mathematics Institute has included it among the seven most important open problems in mathematics and offered 1 million dollars for a proof or counter-example.

2.2 Turbulent flow

Turbulence is a physical phenomenon the fundamentals of which are not yet fully understood. It is a quasi-chaotic time dependent behaviour seen in many fluids, that causes the formation of swirling eddies of different length scales. We can mathematically describe turbulence only in a phenomenological sense – we are not talking about causes but about consequences. Turbulent flow arises in all kinds of problems when the Reynolds number surpasses a certain critical value. Turbulent flows are characterized by fluctuating velocity fields. These fluctuations mix transported quantities such as momentum, energy, and species concentration, and cause the transported quantities to fluctuate as well. Since these fluctuations can be of small scale and high frequency, they are too computationally expensive to be simulated directly, at least in all practical engineering applications. Instead, the instantaneous (exact) governing equations are in some way averaged, to remove the small scales, resulting in a modified set of equations that are computationally less expensive to solve. However, the modified equations contain additional unknown variables, and turbulence models are needed to determine these variables in terms of known quantities (Warnatz et al. 2001).

2.2.1 Influence of turbulence on the governing equations

The fluctuating behaviour of turbulence represents a serious obstacle when modelling turbulent flows. Although turbulence is not as chaotic as we suppose it to be, the assumption of randomness is acceptable and favourable, because it enables us to use statistical methods and approaches. In engineering applications we are not interested in detailed information about turbulent fluctuations but mostly in mean values. That is why various approaches were developed to compute mean values disregarding random fluctuations. The decomposition is typically done as follows:

$$\varphi = \overline{\varphi} + \varphi' , \tag{2.9}$$

where $\overline{\varphi}$ is the time-mean value of the quantity φ and φ' is its instant fluctuation.

Now let us briefly review several basic definitions and rules of work with mean and fluctuating components. The mean value of a scalar φ is defined by:

$$\Phi = \lim_{T\to\infty} \frac{1}{T} \int_0^T \varphi(t) dt . \tag{2.10}$$

The mean value of the fluctuating component is of course equal to zero:

$$\overline{\varphi'} = \lim_{T\to\infty} \frac{1}{T} \int_0^T \varphi'(t) dt = 0. \tag{2.11}$$

If we have two scalars φ, ψ and $\varphi = \Phi + \varphi'$, $\psi = \Psi + \psi'$, the following rules may be shown to be valid:

$$\begin{aligned} &\overline{\frac{\partial \varphi}{\partial s}} = \frac{\partial \Phi}{\partial s}, \quad \overline{\int \varphi ds} = \int \Phi ds \\ &\overline{\varphi + \psi} = \Phi + \Psi, \quad \overline{\varphi\psi} = \Phi\Psi + \overline{\varphi'\psi'}. \end{aligned} \tag{2.12}$$

When we apply the averaging to the Navier-Stokes equations we can derive the so called RANS (Reynolds-averaged Navier-Stokes) equations.

In some flow problems, especially when combustion is considered, there are great changes in density. In this case it is more convenient to use another averaging approach, so-called Favre-averaging. To distinguish from Reynolds-averaging a different notation is used:

$$\tilde{\varphi} = \lim_{T\to\infty} \frac{1}{\overline{\rho} T} \int_0^T \rho\varphi(t) dt, \quad \varphi'' = \varphi - \tilde{\varphi}. \tag{2.13}$$

Whether we use Reynolds- or Favre-averaging, the averaged Navier-Stokes equations contain the following types of unknown terms:

$$\overline{u'v'}. \tag{2.14}$$

Both approaches simplify the governing equations in the sense of replacing fluctuating variables by their mean values but on the other hand they add six new unknowns ($\overline{u'u'}, \overline{u'v'}, \overline{u'w'}, \overline{v'w'}, \ldots$) to the momentum equation (in analogy with viscous stresses, we call them *Reynolds stresses*) and more similar unknowns to other scalar transport equations. Therefore we need additional methods to compute these unknowns. (Warnatz et al. 2001)

2.2.2 Moment closure methods (MCM)

This family of models is the most wide-spread in industrial applications. These models are called MCM because the Reynolds stresses can be viewed as second-order moments of the local probability distribution.

Boussinesq Hypothesis

In 1877 Boussinesq proposed that the Reynolds stresses can be interpreted as gradient transport:

$$\overline{\rho u' q'} = -\rho \nu_t \, grad(\tilde{q}), \tag{2.15}$$

where $q' = u, v, w, \ldots .$

In some cases the turbulent eddy viscosity is used instead: $\mu_t = \rho \nu_t$ instead. This hypothesis often provides a sufficient estimate and is widely used despite being proven wrong in some cases.

Algebraic models

Algebraic models are also called zero-equation models because they do not use any partial differential equation to model the Reynolds stresses. In 1925 Ludwig Prandtl proposed an algebraic equation that approximates the turbulent exchange coefficient using a parameter called *mixing length*. Other modifications of the Prandtl model introduced only different ways to compute the mixing length parameter. All these models use the Boussinesq hypothesis and are used only rarely for very rough estimates.

One equation models

One equation turbulence models solve one turbulence-related transport equation, usually for the turbulent kinetic energy, which is then used to compute the turbulent exchange coefficient by equation (2.15). These models are nowadays used only in very specific cases on simple problems and are almost of no importance except for Spalart-Allmaras model (FLUENT 2005). The Spalart-Allmaras model was designed specifically for aerospace applications involving wall-bounded flows and has been shown to give good results for boundary layers subjected to adverse pressure gradients. It is also gaining popularity in turbomachinery applications. All one equation models again use the Boussinesq hypothesis.

Two equation models

Two equation turbulence models are one of the most common types of turbulence models. Models like the $k-\varepsilon$ model and the $k-\omega$ model have become industry standards and are commonly used for most types of engineering problems. Two

equation turbulence models are still an active area of research and new refined two equation models are still being developed. However, none of the so far proposed models can be branded as being universal.

By definition, two equation models include two transport equations to represent the turbulent properties of the flow. This allows a two equation model to account for history effects like convection and diffusion of turbulent energy.

Most often one of the transported variables is the turbulent kinetic energy k. The transport equation has typically the following form (FLUENT 2005):

$$\frac{\partial}{\partial t}(\rho k) + \nabla \cdot (\rho k \mathbf{v}) = \nabla \cdot \left[\left(\mu + \frac{\mu_t}{\sigma_k} \right) \nabla k \right] + G_k + G_b - \rho\varepsilon - Y_M + S_k . \qquad (2.16)$$

The second transported variable is less well established. Common choices are the turbulent kinetic energy dissipation rate ε or the specific dissipation rate $\omega = \varepsilon/k$. The second variable can also be thought of as the variable that determines the scale of the turbulence (length-scale or time-scale), whereas the first variable k, determines kinetic energy of the turbulent eddies. In case the second variable is ε, the transport equation typically reads (FLUENT 2005):

$$\frac{\partial}{\partial t}(\rho\varepsilon) + \nabla \cdot (\rho\varepsilon \mathbf{v}) = \nabla \cdot \left[\left(\mu + \frac{\mu_t}{\sigma_\varepsilon} \right) \nabla \varepsilon \right] + C_{1\varepsilon} \frac{\varepsilon}{k} (G_k + C_{3\varepsilon} G_b) - C_{2\varepsilon} \rho \frac{\varepsilon^2}{k} + S_\varepsilon . \qquad (2.17)$$

Two equation models also make use of the Boussinesq hypothesis.

Reynolds stress models (RSM)

In some cases we can not neglect the handicaps of the controversial Boussinesq hypothesis; therefore we need to solve transport equations for the Reynolds stresses directly. These equations contain however unknowns interpretable as third order moments. We could derive transport equation for the third order moments but four order moments would arise and so on. This is referred to as the closure problem in turbulence theory. However, physical meaning and measurement of moments of order higher than two is very obscure, which makes such models hard to validate experimentally. Therefore it is preferred to use transport equations “only” for second order moments – Reynolds stresses. (Hájek 2007)

The Reynolds stress model is a higher level, elaborate turbulence model. The exact Reynolds stress transport equation accounts for the directional effects of the Reynolds stress fields. RSM usually solves 6 Reynolds stress transport equations and in addition the ε equation. When compared to two equation models, RSM shows noticeable improvement only in more complex problems, like highly swirling flows.

2.2.3 Direct Numerical Simulation (DNS)

The most accurate way to solve the (non-averaged) Navier-Stokes equations is to solve them directly (numerically of course) without any turbulence model. This means that the whole range of spatial and temporal scales of the turbulence must be resolved. In order to do so we need a very fine mesh. But given the enormously high computational costs, DNS is presently useful only for research purposes.

2.2.4 Large Eddy Simulation (LES)

Turbulent flows are characterized by eddies with a wide range of length and time scales. The largest eddies are typically comparable in size to the characteristic length of the mean flow. The smallest scales are responsible for the dissipation of turbulence kinetic energy. In LES, large eddies are resolved directly, while small eddies are modelled. Large eddy simulation thus falls between DNS and MCM in terms of the fraction of the resolved scales. The main advantage of LES over computationally cheaper RANS approaches is the increased level of detail it can deliver. While RANS methods provide "averaged" results, LES is able to predict instantaneous flow characteristics and resolve turbulent flow structures. This may be particularly important e.g. in simulations involving chemical reactions, such as the combustion of fuel in an engine. While the mean concentration of chemical species or temperature may be too low to trigger a reaction, instantaneously there can be localized areas -in which reactions will occur.

2.2.5 Recent applications

Many recent studies propose combustion models based on “superior” turbulence models (i.e. large-eddy simulation). This brief review is deemed necessary in spite of the obvious complexity and practical inconvenience of such models.

Ferraris and Wen (2007) used a so-called flame index concept for large eddy simulation developed in (Domingo et al. 2002). It was used to capture the partially premixed structure at the leading point and the dual combustion regimes further downstream on a turbulent lifted flame, composed of premixed and nonpremixed flame elements each separately described under a flamelet assumption. They have created a SGS (sub-grid scale) model for partially premixed combustion and implemented it into an existing LES code. Their model is based on the linear coupling of two independent approaches for premixed and nonpremixed combustion through the flame index concept, which uses the fuel and oxygen gradients to detect the combustion regime. When compared with experiments, the model shows good agreement for the lift-off height and the mean mixture fraction. In a similar study (Raman et al. 2005) large-eddy simulation is coupled with Lagrangian filtered-density-function approach in order to model low-Mach-number reacting flows.

The paper by Mahalingam et al. (1995) compares two chemical reaction models by applying them to a three-dimensional direct numerical simulation (DNS) of turbulent nonpremixed flames including finite-rate chemistry and heat release effects. The first model is a single-step global reaction model in which the heat release and activation energy parameters are typical of combustion applications. The second model is a two-step model. The problem investigated involves an initially one-dimensional laminar, unstrained, diffusion flame interacting with a three-dimensional decaying turbulence. Conditions ranging from fast chemistry to pure mixing limit were studied by varying a global Damkohler number. The results suggest that turbulence-induced mixing acting along the stochiometric line leads to a strong modification of the inner structure of the turbulent flame compared with a laminar strained flame, resulting in intermediate species concentration well above the laminar prediction. This result is shown to be consistent with experimental observations.

An interesting comparison study is carried out in (Sanders et al. 1997). In this work emphasis is put on “classical” moment closure turbulence models. The standard

$k-\varepsilon$ model and Reynolds Stress Model are used to investigate variable density effects in axially symmetric turbulent jets. Without buoyancy, both models predict no effect of the varying density on the far field turbulence parameters. Effects of turbulence production due to buoyancy are found to be small compared to the effect of the mean buoyancy term in the momentum equation. However, this turbulence production has a large influence on the axial scalar flux, which is predicted by RSM but not at all with the $k-\varepsilon$ model.

2.3 Reacting flow

The challenge of modelling turbulent reacting flows consists of two interrelated parts, namely the representation of chemical reaction mechanism and its coupling with turbulence. The model descriptions and equations in this section were mostly adopted from (FLUENT 2005) and (Warnatz et al. 2001).

2.3.1 Models using species transport equations

The most straightforward modelling approaches are based on transport equation of individual chemical species. The transport equation for chemical species is given by the following equation:

$$\frac{\partial}{\partial t}\left(\rho Y_i\right)+\nabla\cdot\left(\rho\mathbf{v}Y_i\right)=-\nabla\cdot\mathbf{J}_i+R_i+S_i\,. \tag{2.18}$$

The diffusion flux $\mathbf{J}_i$ is computed using the following form:

$$\mathbf{J}_i=-\left(\rho D_{i,m}+\frac{\mu_t}{Sc_t}\right)\nabla Y_i\,. \tag{2.19}$$

Sc_t is the turbulent Schmidt number defined as $Sc_t=\dfrac{\mu_t}{\rho D_t}$.

The reaction rates that appear in equation (2.18) can be computed by one of the following models – laminar finite-rate model, so-called eddy-dissipation model or so-called eddy-dissipation concept model. In the following three sections these models will be shortly introduced.

Laminar Finite-Rate model

The laminar finite-rate model computes the chemical source terms using Arrhenius expressions, and ignores the effects of turbulent fluctuations. The model is exact for laminar flames, but is generally inaccurate for turbulent flames due to highly non-linear Arrhenius chemical kinetics. The laminar model may, however, be acceptable for combustion with relatively slow chemistry and small turbulent fluctuations, such as supersonic flames.

The net source of chemical species i due to reaction is computed as the sum of the Arrhenius reaction sources over the N_R reactions that the species participate in:

$$R_i = M_{w,i} \sum_{r=1}^{N_R} \hat{R}_{i,r} \ . \tag{2.20}$$

Reaction may occur in the continuous phase between continuous-phase species only, or at wall surfaces.

Consider the rth reaction written in general form as follows:

$$\sum_{i=1}^{N} \upsilon'_{i,r} M_i \underset{k_{b,r}}{\overset{k_{f,r}}{\rightleftharpoons}} \sum_{i=1}^{N} \upsilon''_{i,r} M_i \ , \tag{2.21}$$

where N is the number of chemical species in the system.

Equation (2.21) is valid for both reversible and non-reversible reactions. If the reaction is non-reversible, the backward rate constant is simply omitted.

The forward rate constant for reaction r, $k_{f,r}$, is computed using the Arrhenius expression:

$$k_{f,r} = A_r T^{\beta_r} e^{-E_r/RT} \ , \tag{2.22}$$

where A_r is the pre-exponential factor.

In the case of reversible reaction, the backward rate constant for reaction r, $k_{b,r}$, is computed from the forward rate constant using the following equation:

$$k_{b,r} = \frac{k_{f,r}}{K_r} \ . \tag{2.23}$$

Eddy-Dissipation model

The basic and simplest model for turbulent combustion is the model based on the work of Magnussen and Hjertager – the Eddy-Dissipation model. This model assumes that combustion is "mixing limited". This means that turbulence slowly mixes fuel and oxidizer into reaction zones where they burn quickly. With this assumption it is then safe to substitute chemical kinetic rates by the rates of turbulent mixing.

The net rate of production of species i due to reaction r, $R_{i,r}$, is given by the smaller (i.e., limiting value) of the two expressions below:

$$\begin{aligned} R_{i,r} &= \upsilon'_{i,r} M_{w,i} A \rho \frac{\varepsilon}{k} \min_{\mathrm{R}} \left(\frac{Y_{\mathrm{R}}}{\upsilon'_{\mathrm{R},r} M_{w,\mathrm{R}}} \right) \\ R_{i,r} &= \upsilon'_{i,r} M_{w,i} A B \rho \frac{\varepsilon}{k} \frac{\sum_{\mathrm{P}} Y_{\mathrm{P}}}{\sum_{j}^{N} \upsilon''_{i,r} M_{w,j}} \ . \end{aligned} \tag{2.24}$$

A and B are empirical constants typically equal to 4 and 0,5 respectively and k is the high-pressure limit parameter.

In this model, every reaction has the same turbulent rate. Thus it cannot predict radical species and should be used only with simple one-step or two-step global reaction mechanisms. In equations (2.24), the chemical reaction rate is governed by the large-eddy mixing time scale k/ε. Combustion proceeds whenever turbulence is present ($k/\varepsilon > 0$), and an ignition source is not required to initiate combustion. This also leads to the fact, that ED model is unable to predict flame lift-off.

Eddy-Dissipation Concept Model

The eddy-dissipation concept (EDC) model is an extension of the eddy-dissipation model that includes detailed chemical mechanisms. It assumes that reaction occurs in small turbulent structures, called the fine scales. The length scale of the fine eddies is modelled as:

$$\xi^* = C_\xi \left(\frac{\nu\varepsilon}{k^2} \right)^{\frac{1}{4}}, \tag{2.25}$$

where * denotes fine-scale quantities.

The volume fraction of the fine scales is calculated as ξ^3. Species are assumed to react in the fine structures over a time scale τ given by:

$$\tau = C_\tau \left(\frac{\nu}{\varepsilon} \right)^{\frac{1}{2}}. \tag{2.26}$$

Contrary to the eddy-dissipation model, EDC takes into account the chemical kinetic rates and since it can make use of very complex chemical mechanisms it requires great amount of computational time.

This model can make good use of detailed chemical mechanisms (including hundreds of reactions) and is capable of predicting radical species, pollutant formation and different flame phenomena like lift-off, extinction, etc.

2.3.2 Equilibrium model

When nonpremixed combustion is considered, fuel and oxidizer enter the reaction zone separately in distinct streams. Under specific assumptions, the thermochemistry can be reduced to a single parameter, the mixture fraction. The mixture fraction, denoted by f, is the mass fraction of species that originated from the fuel stream. It may represent the local mass fraction of burnt and unburnt fuel stream elements (C, H, etc.) in all species (CO_2, H_2O, O_2, etc.).

Mixture fraction

The mixture fraction can be written in terms of the atomic mass fraction as:

$$f = \frac{Z_i - Z_{i,ox}}{Z_{i,fuel} - Z_{i,ox}}, \tag{2.27}$$

where Z_i is the elemental mass fraction for element i. The subscript ox denotes the value at the oxidizer stream inlet and the subscript $fuel$ denotes the value at the fuel stream inlet. If we assume the diffusion coefficients for all species are equal, then equation (2.27) is identical for all elements and the mixture fraction definition is universal. While the assumption of equal diffusivities is problematic for laminar flows, it is generally acceptable for turbulent flows where turbulent convection overwhelms molecular diffusion.

This approach is convenient because atomic elements are conserved in chemical reactions. Therefore the mixture fraction can be treated as a conserved scalar quantity, and thus its governing transport equation does not have a source term. The transport equation for the mixture fraction then reads (using Favre-averaging):

$$\frac{\partial}{\partial t}\left(\rho \bar{f}\right) + \nabla \cdot \left(\rho v \bar{f}\right) = \nabla \cdot \left(\frac{\mu_t}{\sigma_t} \nabla \bar{f}\right), \tag{2.28}$$

Additionally a conservation equation for the mixture fraction variance $\overline{f'^2}$ is solved in addition:

$$\frac{\partial}{\partial t}\left(\rho \overline{f'^2}\right) + \nabla \cdot \left(\rho v \overline{f'^2}\right) = \nabla \cdot \left(\frac{\mu_t}{\sigma_t} \nabla \overline{f'^2}\right) + C_g \mu_t \left(\nabla \bar{f}\right)^2 - C_d \rho \frac{\varepsilon}{k} \overline{f'^2} + S_{user}, \tag{2.29}$$

where $f' = f - \bar{f}$. The commonly used values for the constants σ_t, C_g and C_d are 0.85, 2.86 and 2 respectively. S_{user} is a user-defined source term (default value zero). The mixture fraction variance is used in the closure model describing turbulence-chemistry interaction. These two equations apply only for the case where there is one inlet for fuel and one inlet for oxidizer. Nevertheless, the equations can be modified to account for multiple streams.

The power of the mixture fraction modelling approach is that the chemistry description is reduced to two transport equations. Under the assumption of chemical equilibrium, all thermochemical scalars (species fractions, density, and temperature) are uniquely related to the mixture fraction. When taking into account adiabatic systems, the instantaneous values of mass fractions, density and temperature depend only on the instantaneous mixture fraction f:

$$\phi_i = \phi_i\left(f\right), \tag{2.30}$$

where ϕ_i represents the instantaneous species mass fraction, density or temperature. In the case of non-adiabatic systems, the effect of heat loss/gain is parameterized as:

$$\phi_i = \phi_i\left(f, H\right), \tag{2.31}$$

where H is the instantaneous enthalpy.

The turbulent nonpremixed flame problem is now reduced to tracking the turbulent mixing of f. This tracking can be done from wide variety of levels including DNS, LES and RANS.

Modelling of turbulence-chemistry interaction

Equations (2.30) and (2.31) describe the instantaneous relationships between mixture fraction and species fractions, density, and temperature under the assumption of chemical equilibrium. The prediction of the turbulent reacting flow, however, is concerned with prediction of the averaged values of these fluctuating scalars. How these averaged values are related to the instantaneous values depends on the turbulence-chemistry interaction model. One possibility it to apply the assumed-shape probability density function (PDF).

The probability density function, written as $p(f)$, can be thought of as the fraction of time that the fluid spends in the vicinity of the state f. More formally:

$$p(f)\Delta f = \lim_{T\to\infty}\frac{1}{T}\sum_i \tau_i \,, \tag{2.32}$$

where T is the time scale and τ_i is the amount of time that f spends in the Δf band. The shape of the function $p(f)$ depends on the nature of the turbulent fluctuations in f. In practice, $p(f)$ is modelled as a mathematical function that approximates the actual PDF shapes that have been observed experimentally.

The probability density function $p(f)$ can then be used to compute averaged values that depend on f. Density-weighted mean species mass fractions and temperatures can be computed (in adiabatic systems) as:

$$\overline{\phi}_i = \int_0^1 p(f)\phi_i(f)\,df \,. \tag{2.33}$$

Using equation (2.33), it remains only to specify the shape of the function $p(f)$ in order to determine the local mean fluid state at all points of the flow field. One of the functions that are often used in engineering applications is the β-function PDF shape given by the following function of $\overline{f}$ and $\overline{f'^2}$:

$$p(f) = \frac{f^{\alpha-1}(1-f)^{\beta-1}}{\int f^{\alpha-1}(1-f)^{\beta-1}\,df}, \tag{2.34}$$

where

$$\alpha = \bar{f}\left[\frac{\bar{f}\left(1-\bar{f}\right)}{\overline{f'^2}}-1\right]$$
$$\beta = \left(1-\bar{f}\right)\left[\frac{\bar{f}\left(1-\bar{f}\right)}{\overline{f'^2}}-1\right]. \tag{2.35}$$

It is important to notice, that the PDF shape $p(f)$ is a function of only its first two moments, namely the mean mixture fraction $\bar{f}$ and the mixture fraction variance $\overline{f'^2}$. Thus, given the prediction of $\bar{f}$ and $\overline{f'^2}$ at each point of the flow field, the assumed PDF shape can be computed and used as the weighting function to determine the mean values of species mass fractions, density and temperature using equation (2.33).

In real life combustion problem, the assumption of chemical equilibrium is often violated. Therefore when the Equilibrium model is implemented in CFD software, usually there is a possibility to specify species that are known to break the equilibrium assumption and exclude them from the simulation. Of course, the user must determine how such species would affect the desired outcome and if it is safe to neglect them.

2.3.3 Steady Laminar Flamelet model

The steady laminar flamelet approach models a turbulent flame brush as an ensemble of discrete, steady laminar flames, called flamelets. The individual flamelets are assumed to have the same structure as laminar flames in simple configurations, and are obtained by experiments or calculations. Using detailed chemical mechanisms, it is possible to calculate e.g. laminar opposed-flow diffusion flamelets. The laminar flamelets are then embedded in a turbulent flame using statistical PDF methods.

The advantage of the laminar flamelet approach is that realistic chemical kinetic effects can be incorporated into turbulent flames. The chemistry can then be pre-processed and tabulated, offering tremendous computational savings. However, the steady laminar flamelet model is limited to modelling combustion with relatively fast chemistry. The flame is assumed to respond instantaneously to the aerodynamic strain, and thus the model cannot capture deep non-equilibrium effects such as ignition, extinction, and slow chemistry (like NO_x). On the other hand, this model shows great improvements when compared to the equilibrium model in problems where species reactions depart moderately from chemical equilibrium.

Flamelet concept

The flamelet concept views the non-premixed turbulent flame as an ensemble of thin, laminar, locally one-dimensional flamelet structures embedded within the turbulent flow field (see Fig 2-1).

A common laminar flame used to represent a flamelet in a turbulent flow is the counter-flow diffusion flame. This geometry consists of opposed, axi-symmetric fuel and oxidizer jets. When the distance between the jets is decreasing and/or the

velocity of the jets is increasing, the flame is strained and increasingly departs from chemical equilibrium until it is eventually extinguished. The species mass fraction and temperature fields can be measured in laminar counter-flow diffusion flame experiments, or calculated. For the latter, a self-similar solution exists, and the governing equations can be simplified to one dimension along the axis of the fuel and oxidizer jets, where complex chemistry calculations can be affordably performed.

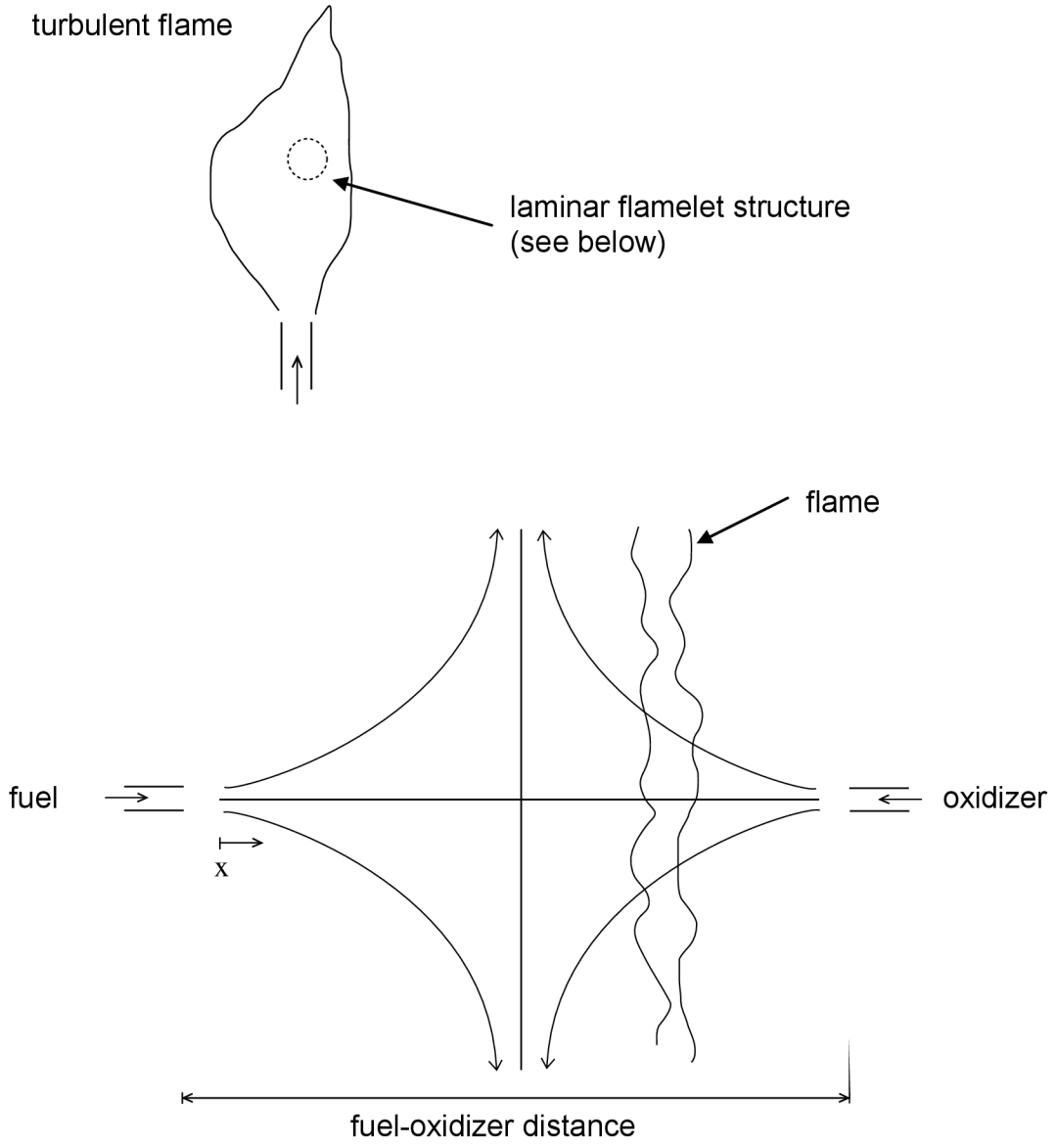

Fig 2-1 *Adopted from (FLUENT 2005)*

In the laminar counterflow flame, the mixture fraction f decreases monotonically from unity at the fuel jet to zero at the oxidizer jet. If the species mass fraction and temperature along the axis are mapped from physical space to mixture fraction space, they can be uniquely described by two parameters: the mixture fraction and the scalar dissipation χ defined as:

$$\chi = 2D\left|\nabla f\right|^2, \tag{2.36}$$

where D is a representative diffusion coefficient. It is important to note, that the scalar dissipation varies along the axis of the flamelet. For the counterflow geometry, the flamelet strain rate a_s can be related to the scalar dissipation at the position where f is stochiometric by:

$$\chi_{st} = \frac{a_s \exp\left(-2\left[\operatorname{erfc}^{-1}\left(2f_{st}\right)\right]^2\right)}{\pi}$$
$$a_s = \frac{v}{2d}, \tag{2.37}$$

where v is the relative speed of the fuel and oxidizer jets, d is the distance between the jet nozzles, χ_{st} is the scalar dissipation at $f = f_{st}$, f_{st} is the stochiometric mixture fraction and erfc^{-1} is the inverse complementary error function.

Physically, as the flame is strained, the width of the reaction zone diminishes, and the gradient of f at the stochiometric position $f = f_{st}$ increases. The instantaneous stochiometric scalar dissipation χ_{st} is used as the essential non-equilibrium parameter. It has the dimensions s^{-1} and may be interpreted as the inverse of a characteristic diffusion time. In the limit $\chi_{st} \to 0$ the chemistry tends to equilibrium, and as χ_{st} increases due to aerodynamic straining, the non-equilibrium increases. Local quenching of the flamelet occurs when χ_{st} exceeds a critical value.

Hence, the chemistry is reduced and completely described by the two quantities f and χ. This reduction of the complex chemistry to two variables allows the flamelet calculations to be pre-processed, and stored in look-up tables. By pre-processing the chemistry, computational costs are greatly reduced.

Embedding Laminar Flamelets in Turbulent Flames

A turbulent flame brush is modelled as an ensemble of discrete laminar flamelets. Since, for adiabatic systems, the species mass fraction and temperature in the laminar flamelets are completely parameterized by f and χ_{st}, density-weighted mean species mass fractions and temperature in the turbulent flame can be determined from the PDF of f and χ_{st} as:

$$\overline{\phi} = \iint \phi\left(f, \chi_{st}\right) p\left(f, \chi_{st}\right) df d\chi_{st}, \tag{2.38}$$

where ϕ represents species mass fractions and temperature.

The variables f and χ_{st} are assumed to be statistically independent, so the joint PDF $p\left(f, \chi_{st}\right)$ can be simplified as $p_f\left(f\right) p_\chi\left(\chi_{st}\right)$. Again, as in the Equilibrium model, β-function PDF shape is used to approximate p_f, and transport equations for $\overline{f}$ and

$\overline{f'^2}$ are solved to specify p_f. Fluctuations in χ_{st} are ignored so that the PDF of χ is simply a delta function: $p_\chi = \delta(\chi - \overline{\chi})$. To speed up computations, the integrations in (2.38) are often pre-processed and stored in look-up tables.

The equilibrium model and the steady laminar flamelet model belong to the family of nonpremixed models. The nonpremixed modelling approach has been specifically developed for the simulation of turbulent diffusion flames with fast chemistry. For such systems, the method offers many benefits over the eddy-dissipation models described in previous sections. The nonpremixed model allows intermediate (radical) species prediction, dissociation effects, and rigorous turbulence-chemistry coupling. The method is computationally efficient in that it does not require the solution of a large number of species transport equations. When the underlying assumptions are valid, the non-premixed approach is preferred over the eddy-dissipation models.

2.3.4 PDF Transport model

An attractive method that avoids the mean reaction rate problem is the statistical approach using the probability density function (PDF). The probability that the fluid at a spatial location $\vec{r}$ has density between ρ and $\rho + d\rho$, velocity in x-direction between v_x and $v_x + dv_x$, velocity in y-direction between v_y and $v_y + dv_y$, velocity in z-direction between v_z and $v_z + dv_z$, temperature between T and $T + dT$ and local composition, which corresponds to mass fractions between w_i and $w_i + dw_i$ is given by:

$$P(\rho, v_x, v_y, v_z, w_1, \ldots, w_{N-1}, T; \vec{r}) d\rho dv_x dv_y dv_z dw_1 \ldots dw_{N-1} dT \,, \tag{2.39}$$

where P is called the probability density function (PDF) and N is the number of species ($w_N = 1 - \sum_{i=1}^{N-1} w_i$).

A normalization condition for the PDF is obtained from the fact, that the overall probability for the system to be somewhere in the whole configuration space has to be 1:

$$\int_0^\infty \int_{-\infty}^\infty \int_{-\infty}^\infty \int_{-\infty}^\infty \int_0^1 \ldots \int_0^1 \int_0^\infty P(\rho, v_x, v_y, v_z, w_1, \ldots, w_{N-1}, T; \vec{r}) d\rho dv_x dv_y dv_z dw_1 \ldots dw_{N-1} dT = 1 \,. \tag{2.40}$$

If the PDF $P(\vec{r})$ is known at some point $\vec{r}$, the means of the local properties can be calculated very easily. For the mean density one obtains:

$$\overline{\rho}(\vec{r}) = \int \rho P(\rho, \ldots, T; \vec{r}) d\rho \ldots dT \,, \tag{2.41}$$

where $\int$ denotes all the integrations. This is *ensemble-averaging*. Thus a sufficiently large number of different realizations must be considered and averaged. In experiments, mean values are obtained by averaging over a large number of time- and space-resolved measurements, obtained at constant experimental boundary conditions.

If the whole PDF is known, the mean reaction rates can be determined by integration. The problem is now, how to determine the PDF. Several different methods have been developed, which are used in various applications.

PDF-Transport Equations

The most elegant way is the solution of the PDF-transport equation. A transport equation for the time behaviour of the PDF can be derived form the reacting Navier-Stokes equations. The main advantage of this method is that the chemistry can be treated exactly (while molecular transport has still to be modelled). The numerical solution of such transport equation is very time consuming. The PDF is approximated by a large number of stochastic particles, which represent different realizations of the flow. The Monte-Carlo methods can be used to solve this problem.

Empirical Construction of PDFs

In this method, PDFs are constructed using empirical knowledge about the shape. Here, the observation that major features of turbulent flow calculations are not sensitive to the exact shape of the PDF is consequently used. A simple way to construct multidimensional PDFs is to assume statistical independence of the different variables. Thus, the PDF can be written as a product of one-dimensional PDFs:

$$P(\rho, T, w_1, \ldots, w_{N-1}) = P(\rho) \cdot P(T) \cdot P(w_1) \cdot \ldots \cdot P(w_{N-1}). \tag{2.42}$$

Of course, the assumption of independence is not correct, because T and ρ are generally dependent due to the ideal-gas law. Therefore additional correlations between variables have to be accounted for.

The PDF transport model, like the EDC model, should be used when simulating finite-rate chemical kinetic effects in turbulent reacting flows. With an appropriate chemical mechanism, kinetically-controlled species such as CO and NO_x, as well as flame lift-off, extinction and ignition can be predicted. PDF transport simulations are computationally expensive; therefore this model is used mostly for 2D problems.

2.3.5 Recent applications

In the past few decades many different models for combustion have been proposed. Unfortunately none of these can be thought of as universal, meaning that the use of one model can not cover the majority of industrial applications and give good results. Therefore the present models are studied and compared with experiments, to provide the end-user with important knowledge about limitations and applicability of the model, and new models are still often being proposed.

One of the approaches when dealing with nonpremixed lifted flames, is to take into account the fact that the fuel and oxidizer are already partially mixed. Chen et al. (2000) proposes a flamelet model for turbulent lifted jet flames. The model combines older flamelet models for nonpremixed and premixed combustion and makes use of the so called triple-flame configuration. Chen also proposes a new model for the turbulent burning velocity in partially premixed flows that is based on a formulation for a conditional turbulent burning velocity which depends on mixture fraction. The effect of partial premixing is taken into account by using the presumed probability density

function (PDF) approach in terms of the mixture fraction. From a computational point of view, the model has the advantage that the calculation of the chemical processes can be decoupled from the flow calculation, allowing for simulation of realistic configurations, yet retaining detailed chemistry. Chen also compares lift-off heights computed by his model with experimental data form various authors and finds good agreement.

Norris and Pope (1995) used the velocity dissipation composition probability density function transport approach to model a turbulent $CO/H_2/N_2$ – air-piloted jet diffusion flame in the region of extinction. They reported, that the PDF method predicts flame extinction at approximately the same jet velocity as that of the experiment.

In the paper (Jones and Kakhi 1998) the authors predict the evolution of a piloted methane-air turbulent diffusion flame by applying the joint-scalar probability density function (PDF transport) approach. Their objective is to investigate whether the current PDF approach can treat extinction and reignition phenomena and accurately predict the concentration of species such as CO and H_2. They put to test two different mixing models – coalescence-dispersion and linear mean square estimation (LMSE) – together with two turbulence models – $k-\varepsilon$ and full Reynolds stress. The predictions demonstrated that in general the mixing and fuel consumption rates were well represented. Other scalars such as H_2O and temperature were also satisfactorily predicted for the flame not subjected to local extinction. The LMSE model predicted well the local flame extinctions while with the coalescence-dispersion model stable burning was reproduced though the low temperatures observed were not predicted.

The PDF transport approach is also used in the study of Taing and Masri (1993). He incorporates a simple three-step chemical mechanism in the solution of the joint velocity-composition PDF transport equation and finds out that the computed flame length and radial spread rate agree with experiments. The computed reactive scalars agree with experiments only when the chemical kinetic effects are small to moderate. On the other hand, when the chemical kinetic effects are significant, deviations between measurement and calculation occur.

2.4 Numerical approach

2.4.1 What is CFD?

Computational fluid dynamics (CFD) is one of the branches of fluid mechanics that uses numerical methods and algorithms to solve and analyze problems that involve fluid flows. CFD is often (improperly) identified with computational software for solving various flow problems. The computational software used in this thesis is FLUENT 6.3.26. It is a complex modelling software that can be used in a great variety of flow applications ranging from air flow over an aircraft wing to combustion in a furnace, from bubble columns to oil platforms, from blood flow to semiconductor manufacturing, and from clean room design to wastewater treatment plants.

Most of the CFD software, including FLUENT, work with the governing equations by means of FMV – Finite Volume Method.

2.4.2 Finite-volume method

The finite-volume method (FVM) is a method for representing and evaluating partial differential equations as algebraic equations. Similar to the finite difference method, values are calculated at discrete points on a meshed geometry. "Finite volume" refers to the small volume surrounding each node point on a mesh. In the finite volume method, volume integrals in a partial differential equation that contain a divergence term are converted to surface integrals, using the divergence theorem.

$$\iiint_V div\,\mathbf{F}\,dV = \iint_{\partial V} \mathbf{F}\cdot\mathbf{n}\,dS\,, \tag{2.43}$$

where V represents a volume which is compact and has a piecewise smooth boundary ∂V and $\mathbf{F}$ is a continuously differentiable vector field in the vicinity of V.

These terms are then evaluated as fluxes at the surfaces of each finite volume. Because the flux entering a given volume is identical to that leaving the adjacent volume, these methods are conservative. Another advantage of the finite volume method is that it is easily formulated to allow for unstructured meshes.

2.4.3 Solvers

When solving a flow problem in FLUENT, it is possible to choose from two numerical methods: pressure- and density-based solver. Historically speaking, the pressure-based approach was developed for low-speed incompressible flows, while the density-based approach was mainly used for high-speed compressible flows. However, in the course of time, these methods have been extended and reformulated to solve and operate for a wide range of flow conditions beyond their traditional or original intent.

In both methods the velocity field is obtained from the momentum equations. In the density-based approach, the continuity equation is used to obtain the density field while the pressure field is determined from the equation of state. On the other hand, in the pressure-based approach, the pressure field is extracted by solving a pressure or pressure correction equation which is obtained by manipulating continuity and momentum equations.

Using either method, Fluent will solve the governing integral equations for the conservation of mass and momentum, for energy and other scalars such as turbulence and chemical species. In both cases a control-volume-based technique is used that consists of the following steps:

- Division of the domain into discrete control volumes using a computational grid.
- Integration of the governing equations on the individual control volumes to construct algebraic equations for the discrete dependent variables ("unknowns") such as velocities, pressure, temperature, and conserved scalars.
- Linearization of the discretized equations and solution of the resultant linear equation system to yield updated values of the dependent variables.

The two numerical methods employ a similar discretization process (finite-volume), but the approach used to linearize and solve the discretized equations is different.

Pressure-based solver

In case the pressure-based approach is chosen, either the segregated or coupled algorithm can be applied. The segregated algorithm solves all governing equations sequentially (one after another). Because the equations are non-linear and coupled, the solution loop must be carried out iteratively in order to obtain a converged numerical solution. Each governing equation, while being solved, is "decoupled" or "segregated" from other equations. The segregated algorithm is memory-efficient, since the discretized equations need only be stored in the memory one at a time. However, the solution convergence is relatively slow, inasmuch as the equations are solved in a decoupled manner.

The main difference between the coupled and segregated algorithm is that the coupled algorithm does not decouple the momentum and continuity equations. But all the remaining equations are again solved in a decoupled manner as in the segregated algorithm. Since the momentum and continuity equations are solved in a coupled manner, the rate of solution convergence significantly improves when compared to the segregated algorithm. However, the memory requirement increases.

Density-based solver

The density-based solver solves the governing equations of continuity, momentum, energy and species transport simultaneously – in a coupled manner. Governing equations for additional scalars will be solved afterward and sequentially. Because the governing equations are again non-linear (and coupled), several iterations of the solution loop must be performed before a converged solution is obtained (FLUENT 2005).

3 State of the art

As mentioned in section 1.2, the problem considered in this thesis is a methane-air diffusion flame in a small scale. This specific problem is only one of many, more or less similar, combustion problems that are being tackled in contemporary combustion science and industry.

Combustion of various gaseous fuels under turbulent flow conditions occurs in many engineering applications. In the past few decades, due to significant progress in computer technology, it was possible to introduce different models that describe more or less precisely various combustion phenomena such as flame ignition and extinction, flame stability, pollutant formation, etc.

For the understanding of the following text it is essential to introduce some basic notions. A flame is said to be attached if the combustion process begins immediately as the fuel (or mixture of fuel and oxidizer in the premixed case) exits the nozzle. When combustion starts later and farther from the nozzle orifice we call the flame lifted. Often it is possible to change between these flame regimes, for example by increasing/decreasing fuel exit velocity or by changing the position of igniter. When and attached flame switches to the lifted regime (typically due to an intermittent instability), we call it lift-off. When we have a lifted flame and further increase velocity, usually at some point the flame extinguishes. This is called blowout. Under certain circumstances, when we have an attached flame and increase fuel inlet velocity, extinguishing of the flame occurs before lift-off can even occur – in this case we speak of blowoff.

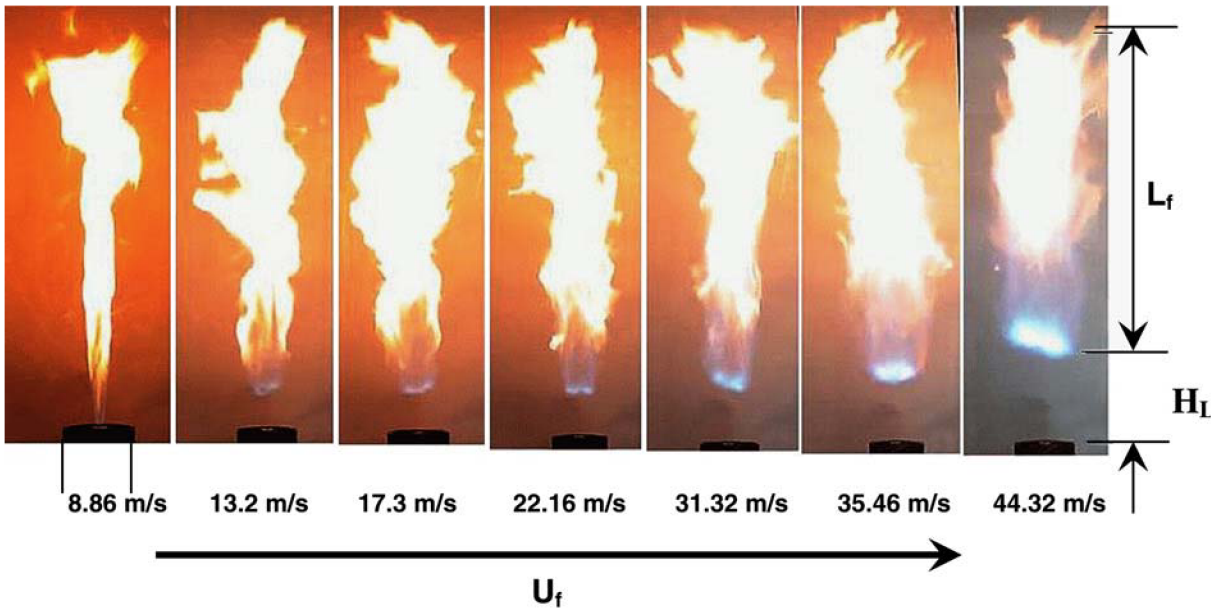

Fig 3-1 *Example of flame lift-off depending on fuel inlet speed (Kiran, Mishra 2007)*

Flame stability

An extensive study performed by Lawn (2009) reviews three principal theories for the stabilization of lifted flames (premixed model, extinction model, large eddy model) in the light of the most recent flame imaging experiments in literature. Similarity solutions for jets in co-flow are developed and new data for lifted flames on methane

jets in diffusing streams of co-flowing air are presented. The study presents a hypothesis that explains how ignition is maintained in experiments with low turbulent lift-off. Lawn supposes that the mechanism is the diffusive heating of the slowly moving surrounding air which then provides an energy store for the incoming eddies.

In many practical combustion systems a co-flow air stream is often added to increase the efficiency of the combustion process, shorten the flame length and reduce the residence time for NO_x formation. However, it has been shown that a very small increase in the co-flow stream velocity can lead to a very dramatic decrease in the lifted flame blowout limit and a lifted flame can only be stabilized at low co-flow velocities (Muniz and Mungal 1997). Leung and Wierzba (2009) investigated experimentally the stability of nonpremixed jet flames in co-flowing air stream. The experimental data they obtained indicate that there exists a range of co-flow velocity where two distinctly different extinction limits can occur at the same co-flow velocity depending on whether the flame is lifted or attached at ignition. The results furthermore show that co-flow velocity has a much greater effect on the blowout limits of lifted flames than on the blowout limits of attached flames. As a part of their study a model predicting lifted flame blowout limits has been developed and it showed very good agreement with experimental data.

A similar experimental study was carried out by Kiran and Mishra (2007). In this study were measured lift-off height, flame length and blowoff velocity of simple LPG (liquefied petroleum gas) jet diffusion flames. It was observed that lift-off height is proportional to the fuel exit velocity. Two regimes identified either as buoyancy or momentum dominated, were characterized by Froude number.

In the paper (Otakeyama et al. 2009) it is also shown that the flame stabilization mechanism is influenced also by the rim thickness.

In engineering practice it is often of great interest under which conditions flame blowout may occur. An experimental study of the blowout mechanism on a turbulent jet diffusion flame is performed in the paper (Wu et al. 2006). The blowout process is categorized into four characteristic regions: pulsating, onset of receding, receding and extinction. Based on experimental findings, a blowout mechanism is proposed based on the triple flame and stochiometric contour. The mechanism also provides an explanation for the fact that the blowout process of a turbulent jet diffusion flame can be estimated and characterized based on the initial velocity and gas properties at the jet exit without knowing the local flame/flow conditions of the lift-off flame near blowout.

Another interesting phenomenon is that of reignition. The paper (Torii et al. 2002) experimentally investigates the morphology of high speed hydrogen jet diffusion flames with emphasis on the flame reignition phenomenon that occurs before the flame blowoff. It concludes that reignition only occurs at certain mass flow rates.

Extinction and reignition phenomena are also treated by Hamins et al. (2007). Hamins investigates the structure and extinction of low-strain nonpremixed flames through comparison of experiments and numerical simulations in both normal gravity and microgravity. The suppression effectiveness of a suppressant N2 added to the fuel stream was measured. A two-dimensional flame simulation, including buoyancy effects, was developed and was validated with the flame suppression and

temperature profile measurements. The 2D model calculations also showed agreement with experimental observation of the flame curvature.

Many papers deal with the flame extinction phenomena. An experimental and computational study (Lock et al. 2007) examined the extinction characteristics of partially premixed flames and nonpremixed flames in co-flow and counter-flow configurations using the chemically inert fire suppressant agent CO_2. The goal of the study was to characterize the relative effectiveness of fuel-stream dilution versus air-stream dilution in extinguishing laminar methane-air flames. Both measurements and simulations show that both fuel and air stream dilution has great effect on flame stability of premixed and nonpremixed flames. Despite different configurations, there is remarkable similarity in the extinction characteristics of co-flow and counter-flow flames with regard to the level of partial premixing and air- and fuel-stream dilution. In (Chao et al. 2004) effect of dilution is demonstrated on the blowout mechanism.

Many of the previously mentioned studies overlooked heat losses due to radiation. The effect of radiation is rather exceptionally taken into account and typically only via a relatively simple approach based on the optically thin flame assumption. Mahmud et al. (2007) published an experimental and computational study that investigates a lifted, free turbulent nonpremixed methane jet flame issuing into quiescent air. They compared the optically thin flame radiation model (OTFRM) with the discrete transfer model (DTRM) and concluded that in the near burner region the temperature predictions are very similar and are in good agreement with measurements. Further downstream the heat loss due to radiation becomes more significant and therefore the predictions using the OTFRM, unlike DTRM, over predicted the heat loss due to radiation and hence, the temperature is under predicted.

4 Experiment and measurements

4.1 Preliminary experiment

The first measurement was held in the laboratories of the Process engineering department. During this measurement our only goal was to select a nozzle diameter of the free jet and methane inlet overpressure such that the flame would be stable and suitable for simulations. We tested three nozzles with diameters 1, 1.5 and 2 mm at various methane overpressures ranging from 0,3 to 0,9 kPa. The methane flow rate was controlled using valves and pressure regulators. In order to minimize room disturbances we put three improvised panels around the burner leaving only one open side for being able to take photographs. The results of this measurement can be seen in Tab 4-1.

After these measurements we decided to use the 2 mm diameter and 0,5 kPa methane overpressure. The reason is that with these settings we were able to get both the attached and lifted flame in a relatively stable configuration (see Fig 4-2 and #10 and #11 in Tab 4-1).

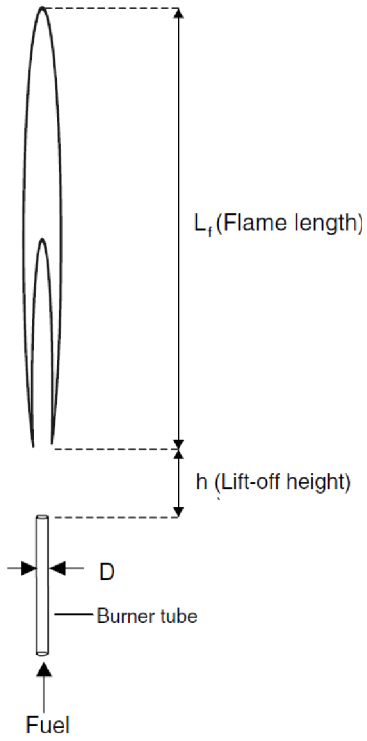

Fig 4-1 *(Mahmud et al. 2007)*

Tab 4-1 *Measurement results*

#	D [mm]	p [kPa]	h [mm]	L_f [mm]	Comments
1	1	0,4	0	150	Smooth laminar flame, blue flame base and yellow flame
2	1	0,5	0	170	Similar to #1, top of the flame exhibits flittering. When disturbed, switches to #3
3	1	0,5	40	100	Very unstable, extinguishes
4	1	0,6	0	200	Similar to #2, but when disturbed blows off
5	1,5	0,4	40	250	Stable, does not hold in attached mode
6	1,5	0,5	50	200	Same as #5
7	1,5	0,6	50	200	Highly unstable, blows out immediately

8	2	0,3	0	350	Similar to #2
9	2	0,4	0	350	Similar to #8
10	2	0,5	0	400	Stable flittering attached flame
11	2	0,5	50	300	Turbulent flame base, flame top smoothly flitters
12	2	0,6	50	300	Similar to #11
13	2	0,7	60	300	Similar to #12
14	2	0,8	70	300	Similar to #12
15	2	0,9	80	300	Very unstable, extinguishes

D – nozzle diameter, p – methane overpressure, h – length of flame lift-off, L_f – flame length

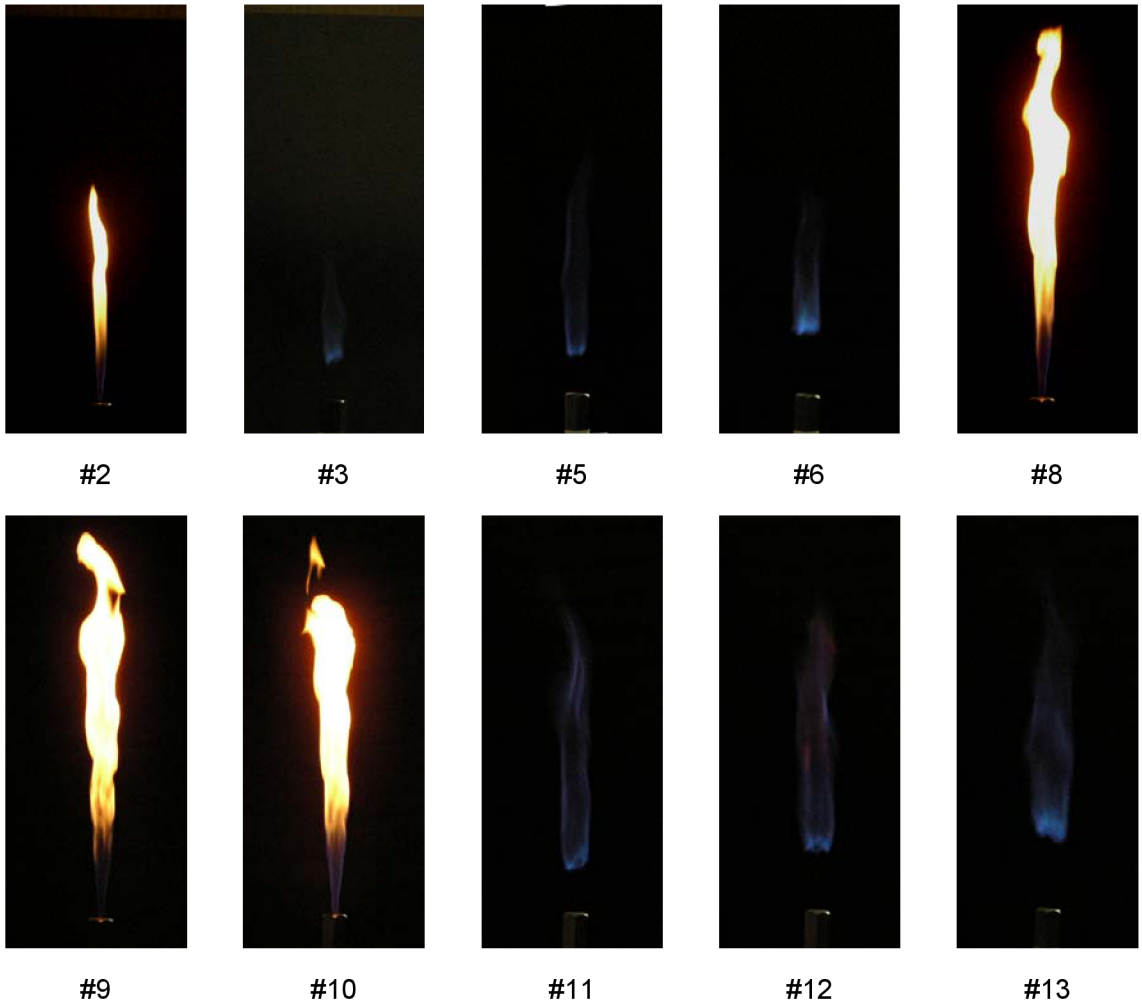

Fig 4-2 *Flames from the preliminary experiment. Numbers refer to Tab 4-1*

4.2 Spectrometric experiment

The second measurement was carried out in the laboratories of the Faculty of Chemistry. The scope of this experiment was to perform a spectrometric measurement of the flame using the configuration chosen in the preliminary experiment (2 mm nozzle diameter and 0,5 kPa methane overpressure). A thermal camera and a high speed camera were available as well. To facilitate the minimizing of room disturbances a moveable construction of thin metal panels was constructed. Unfortunately the disturbances in the laboratory were much bigger than we expected, probably due to the lab air conditioning system. Not only we were unable to reproduce the pre-selected attached flame, but we had also problems stabilizing the lifted flame. To fully utilize the measurement devices it was decided to perform measurements not only at 0,5 kPa methane overpressure, but also at 0,2 kPa methane overpressure. The flame characteristics are shown in Tab 4-2.

Tab 4-2 *Measurement results*

#	D [mm]	p [kPa]	h [mm]	L_f [mm]	$\dot{m}$ [kg/s]	Comments
1	2	0,2	0	270-350	4,25e-5	Stable and fluttering
2	2	0,2	20-30	250-300	4,25e-5	Relatively stable
3	2	0,5	25-35	250-300	5,97e-5	Unstable due to room disturbances

As a part of this measurement, the methane mass flow rates were computed using a chronograph and a flow meter.

The spectrometric measurement (optical emission spectrometry) was performed using an optical spectroscope sequentially placed at various heights (1, 6, 11, 16, 21, 26 cm) facing the nozzle axis. The schematics can be seen in Fig 4-3.

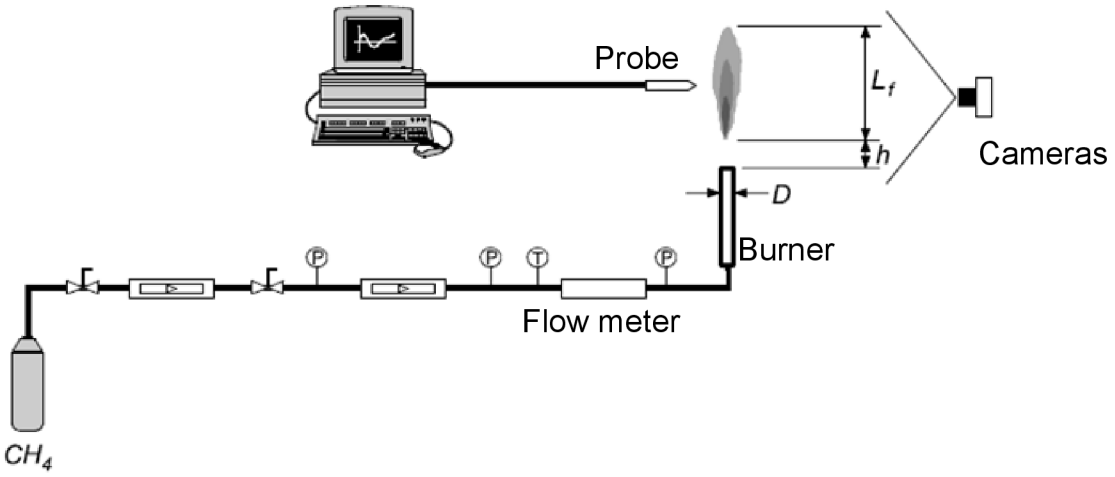

Fig 4-3 *Schematic of the experimental setup (cameras used: high speed, thermal)*

4.2.1 Spectrometric results

The spectrometric data were collected only for configuration #1 and #2 (see Tab 4-2). The configuration #3 was not stable enough to make the spectrometric measurement possible. The data evaluation was carried out by doc. RNDr. František Krčma, Ph.D. from the Faculty of Chemistry. The results presented here are taken from his report.

The yellow attached flame (#1) emits continuous radiation which corresponds to the black body radiation at various temperatures. The lifted blue flame (#2) radiation is emitted by bi-atomic molecules, mainly by the CH excitation (corresponding wavelength is equal to 431,5 nm, which matches the blue flame colour). In the visible spectrum there is also radiation emitted by C_2 molecules (wavelength 516,5 nm – green colour). In the invisible spectrum is detected the OH radical radiation (wavelength 305 nm). The blue flame emits almost no continuous radiation. In the configuration #1 intensity of these spectra diminishes with the rising distance from the nozzle exit, in the configuration #2 the spectral intensity behaves in the same way, but at higher distances is replaced by radiation of molecular water (infrared spectrum).

During the transition form the attached to the lifted flame it is possible to observe both molecular and continuous radiation.

For the dependence of intensities on axial distance from nozzle exit (see Tab 4-4 and Tab 4-5), the wavelengths corresponding to the most intense parts of the respective spectrum (see Tab 4-3).

Tab 4-3 *Corresponding wavelengths*

OH	308,8 nm
CH	430,8 nm
C_2	516,1 nm
H_2O	813 nm

Tab 4-4 *Intensities dependence for configuration #1, uncertain values are marked "?"*

Distance from nozzle exit [cm]	OH intensity	CH intensity	C_2 intensity
1	155	470	670
6	135	440	550
11	85	155	200
16	55	110	400?
21	40?	100?	?
26	20?	60?	?

The noticeable drop in C_2 intensity (see Tab 4-4) is apparently caused by further oxidation of this molecule. Moreover, at higher distances is the radiation disguised by the continuous radiation of the yellow flame.

Tab 4-5 *Intensities dependence for configuration #2, uncertain values are marked "?"*

Distance from nozzle exit [cm]	OH intensity	CH intensity	C_2 intensity	H_2O intensity
1	?	?	?	?
6	410	560	950	120
11	205	235	475	380
16	130	110	150	300
21	90	?	30?	220
26	55	?	?	155

At the 1 cm distance from nozzle exit there is almost no radiation due to the flame lift-off (see Tab 4-5).

If possible, the so-called rotational temperatures were computed using the molecular spectra. The rotational temperature is defined as the temperature corresponding to the Boltzmann-distribution among the rotation-states of molecules. The rotational temperature should agree with the temperature of a neutral gas, where no new particles are arising – which is unfortunately not true in our case. For the rotational temperature calculation rotational spectra in Fig 4-4 and Fig 4-5 have been used. The computed rotational temperatures can be found in Tab 4-6 and Tab 4-7.

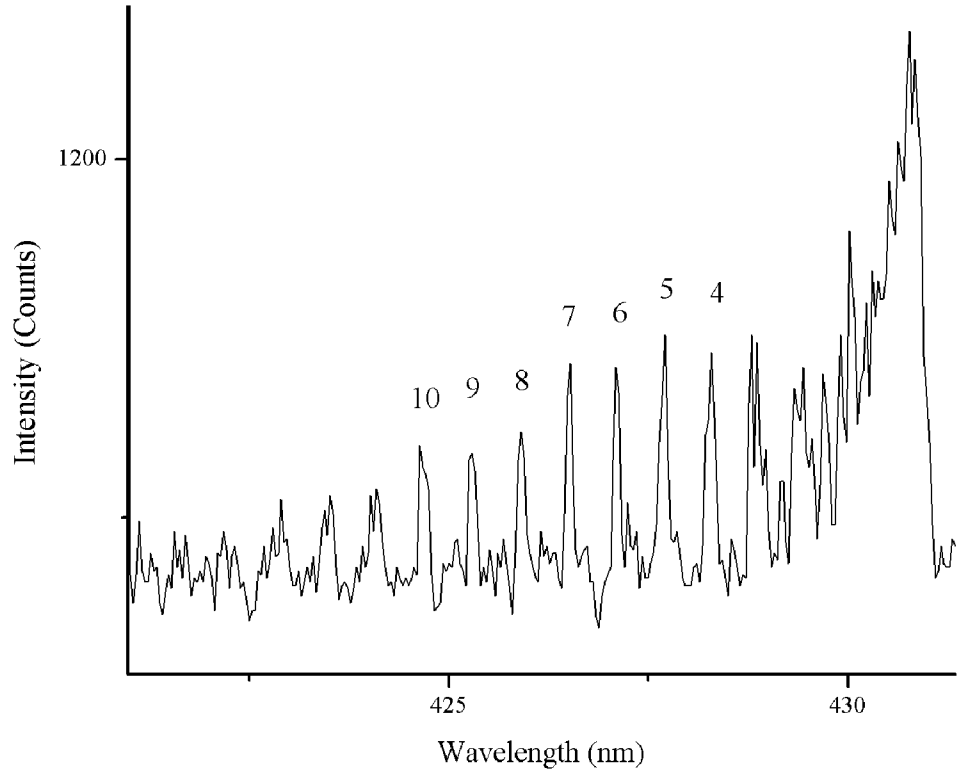

Fig 4-4 *CH rotational spectrum*

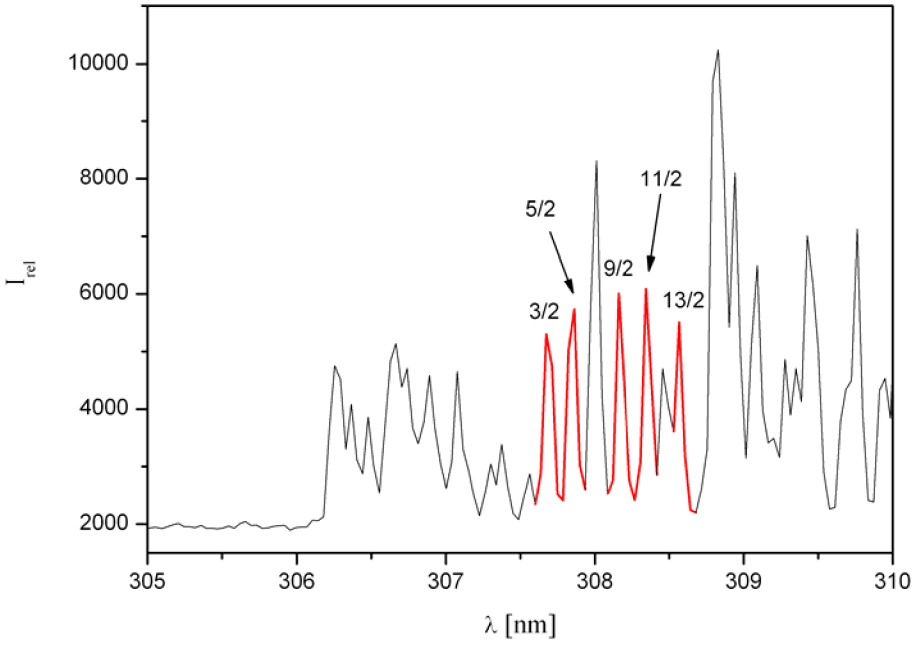

Fig 4-5 *OH rotational spectrum*

Tab 4-6 *Rotational temperatures for configuration #1, uncertain values are marked "?"*

	CH		OH	
Distance from nozzle exit [cm]	Value [K]	Error	Value [K]	Error
1	1260	46	954	200
6	1296	40	803	126
11	1406	157	712	55
16	1796	256	1121	372
21	?	?	592?	174?
26	?	?	?	?

Tab 4-7 *Rotational temperatures for configuration #2, uncertain values are marked "?"*

	CH		OH	
Distance from nozzle exit [cm]	Value [K]	Error	Value [K]	Error
1	?	?	?	?
6	851	133	870	230
11	2180	354	945	262
16	1667	192	873	207
21	?	?	868	164
26	?	?	651	103

4.2.2 Thermal and high speed camera data

The data obtained from the high speed camera were basically of no immediate use but they vividly illustrate the turbulent mixing and burning phenomena. The recording of the lifted flame regime did not quite pay off, since to capture the phenomena one needs a very high frame rate, which was not possible due to the low luminosity of the blue flame. On the other hand, the attached regime and its yellow flame made possible the use of sufficiently high frame rate – 6000 frames per second (fps).

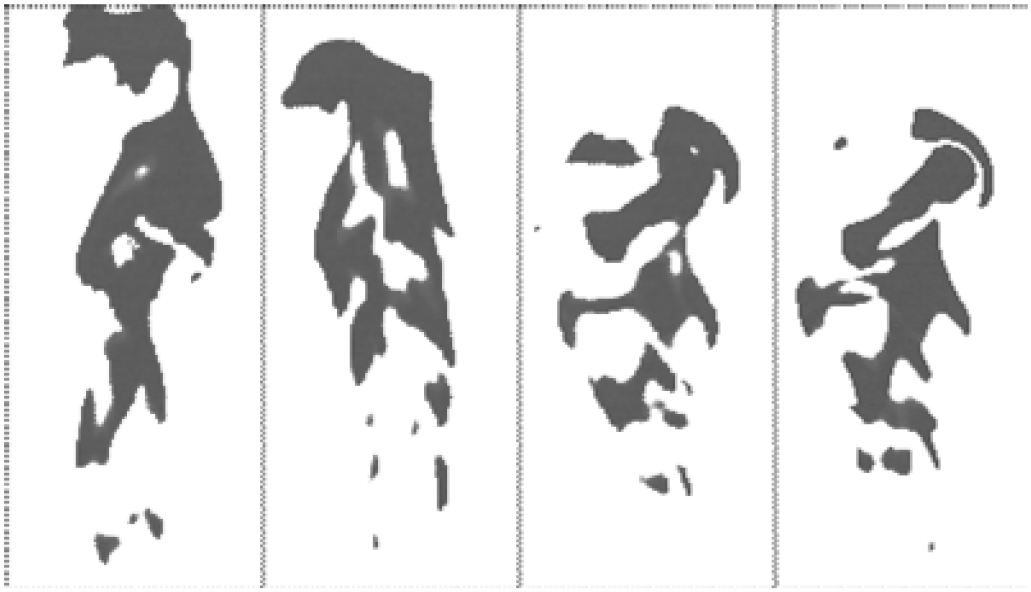

Fig 4-6 *Illustrative frames form the high speed camera recording (edited in GIMP)*

The thermal camera recording gave us a glimpse of the temperature contours, but since thermal cameras are designed for solid materials, the measured temperatures were hardly a good guess. Flame radiation intensity was (as expected) too weak as compared to solid surfaces, therefore the temperatures observed by the camera (max 200°C) deeply underestimated the real flame temperatures (up to 2000°C)

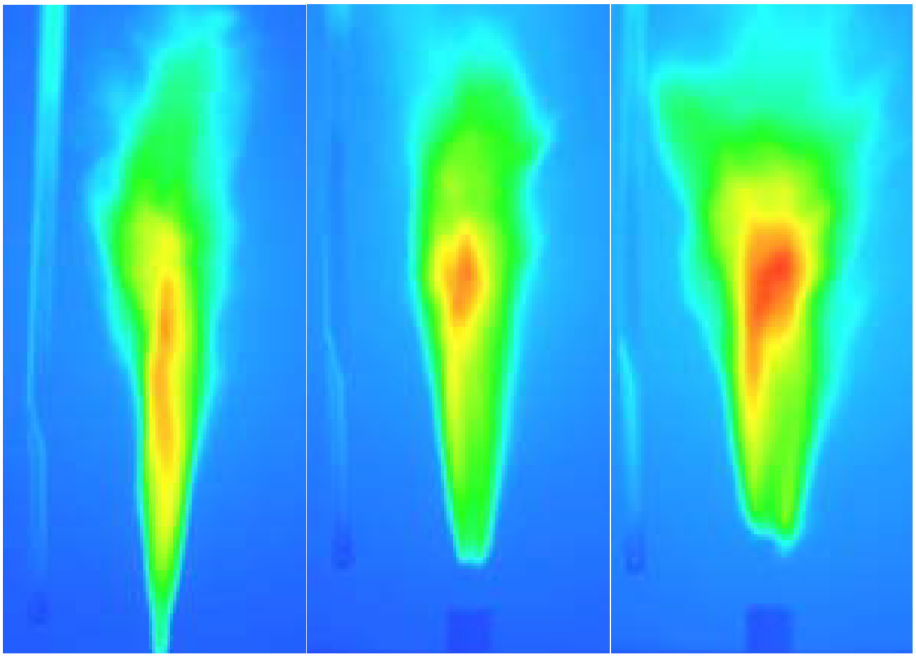

#1 #2 #3

Fig 4-7 *Temperature contours obtained form the thermal camera. Numbers refer to* ***Tab 4-2***

Fig 4-8 *Illustrative photographs of devices used in the spectrometric experiment*

5 Simulations

The grid and mesh files needed for the computations were generated using the software GAMBIT. All the computations were performed by the software FLUENT (version 6.3.26). The computational models mentioned above were used to simulate a nonpremixed unconfined free jet flame, where the fuel (methane) exits into air at atmospheric pressure (101325 Pa). In the simulations, a small air co-flow was added to provide sustainable oxygen supply and represent natural draft in the experimental stand. The temperature of both methane and air were equal to ambient temperature 20°C. Also, the gravitational acceleration was considered (9,81 m/s^2).

All the computations were performed using the two dimensional, double precision, pressure-based, axisymmetric solver.

5.1 Models used

5.1.1 Turbulence models

In the so-called "cold run" simulation, where no chemical reactions but only species mixing is taken into account, I compared 5 basic turbulence models. All the models were used with their default settings (namely their empirical parameter values).

k-ε standard model

The $k-\varepsilon$ standard model is the best known two-equation turbulence model which is used in engineering applications. It is a semi-empirical model that solves 2 partial-differential transport equations for the turbulence kinetic energy k and its dissipation rate ε (see equations (2.16) and (2.17)).

The turbulent viscosity μ_t is computed combining k and ε as follows:

$$\mu_t = \rho C_\mu \frac{k^2}{\varepsilon}. \tag{5.1}$$

k-ε RNG

The RNG model was derived using a rigorous statistical technique called renormalization group theory. This model is similar to the previous one, but it includes certain refinements:

- The RNG model has an additional term in its ε equation that significantly improves the accuracy for rapidly strained flows.
- The effect of swirl on turbulence is taken into account.
- The RNG theory provides an analytical formula for turbulent Prandtl numbers, while the standard model uses user-specified constant values.
- While the standard model is a high-Reynolds-number model, the RNG theory accounts for low-Reynolds-number effects.

k-ε realizable

The realizable model is a relatively recent development and differs from the standard model in two important ways. It contains a new formulation for the turbulent viscosity (it is no longer a constant) and it has a new equation for the dissipation rate that has been derived from an exact equation for the transport of the mean-square vorticity fluctuation.

The term "realizable" means that the model satisfies certain mathematical constraints on the Reynolds stresses, consistent with the physics of turbulent flows. Neither one of the two previously mentioned models are generally physically realizable (it can happen that at certain strain values, quantities that by definition must be positive become negative). One of the benefits of this property is that this model predicts more accurately the spreading rate of jets.

k-ω standard

In FLUENT, the $k-\omega$ standard model is based on the Wilcox $k-\omega$ model, which incorporates modifications for low-Reynolds-number effects, compressibility, and shear flow spreading. This model is an empirical model based on two transport equations – one for the turbulent kinetic energy k and one for the specific dissipation rate ω, $\omega = \varepsilon / k$.

In this model the turbulent viscosity μ_t is calculated as follows:

$$\mu_t = \alpha^* \frac{\rho k}{\omega}. \tag{5.2}$$

RSM

The Reynolds stress model is the most elaborate turbulence model that FLUENT provides. Abandoning the Boussinesq hypothesis, the RSM closes the Reynolds-averaged Navier-Stokes equations by solving transport equations for the Reynolds stresses, together with an equation for the dissipation rate. Due to the increased amount of transport equations to solve, RSM is appreciably more computationally expensive than the two-equation turbulence models. Its advantages can fully show up when dealing with flow features that are the result of anisotropy in the Reynolds stresses. Among the examples are cyclone flows, highly swirling flows in combustors, rotating flow passages, and the stress-induced secondary flows in ducts.

5.1.2 Chemistry models and reaction mechanisms

All models introduced in section 2.3 were used in the simulations. Each model was applied with its default settings and used consistently with the FLUENT's recommended solution procedures.

Reaction mechanisms

Reaction mechanisms can be interpreted as a set of chemical equations (with additional data about species and reaction properties) for various combustion processes. FLUENT provides us with a vast variety of such mechanisms for various fuels, but they are mostly global, which means that they include only a handful of reactions between intermediate species. Global mechanisms usually include one, two or three reactions. Fortunately, FLUENT allows us to import more detailed

reaction mechanisms in CHEMKIN format. This file format is widely used in the scientific community to distribute detailed reaction mechanism data.

In the simulations I used four different reaction mechanisms:

- Gri-MECH 3.0 mechanism for hydrocarbon combustion, 53 species, 325 reversible reactions (Smith et al. 2009)
- Kee mechanism for methane oxidation. 18 species and 58 reversible reactions. From Table B.2 on p. 263 in (Peeters 1995).
- Smooke mechanism for methane combustion. 17 species and 46 reversible reactions. From Table 7 on p. 1787 in (Smooke 1986).
- Reduced (Skeletal) mechanism for methane oxidation. 17 species and 25 reversible reactions (35 reactions if the forward and backward steps are counted separately). From the Table on p. 161 in (Smooke, 1991).

The Gri-MECH mechanism is indeed the most detailed one. It is an optimized detailed chemical reaction mechanism capable of the best representation of natural gas flames and ignition that is presently available and is usually used to compare performances of simpler mechanisms.

When working with the eddy-dissipation model detailed reaction mechanisms are useless. Due to its simplicity and dismissal of chemical kinetic rates, this model can not predict intermediate species and thus makes use only of basic global reaction mechanisms. In the simulation two global mechanisms were used – a one-step ($CH_4+2O_2 \rightarrow 2H_2O+CO_2$) and a two-step mechanism ($CH_4+1.5O_2 \rightarrow CO+2H_2O$, $CO+0.5O_2 \rightarrow CO_2$).

On the other hand, when employing EDC model, PDF transport model, laminar finite-rate model or Steady laminar flamelet model, the use of detailed chemical mechanisms is well-founded and necessary.

5.2 Grid

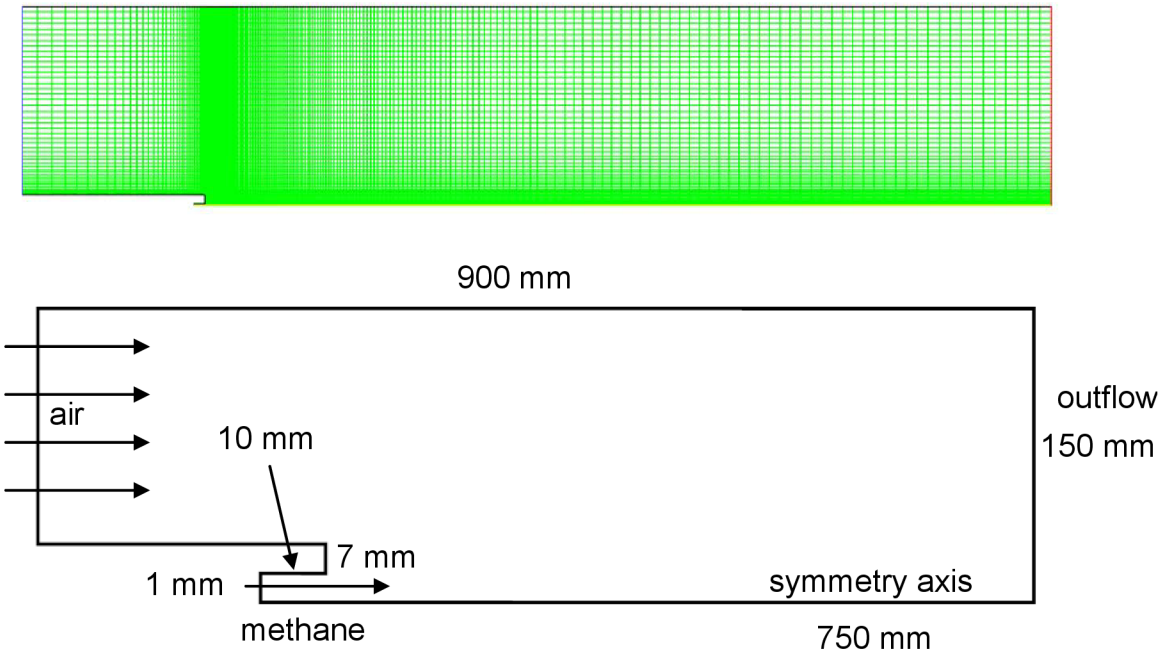

Fig 5-1 *Mesh generated in Gambit and dimensions of the computational domain*

The grid displayed in Fig 5-1 was used in all the simulations.

Since the simulations were performed in 2-D I could afford to generate a very fine mesh. This was also the reason that during the computations there was only little difference between first- and second-order discretization schemes.

5.3 Material properties

All handled materials were fluids. Although the methane and air velocities were not high enough to make compressibility effects relevant, the densities were calculated using the ideal-gas equation instead of using the incompressible-ideal-gas equation. Whenever possible, the constant-pressure specific heats of materials were set to piecewise-polynomial (in the next part it will be shown that a simplification to a constant would seriously distort predicted temperature values).

5.4 Boundary conditions

To be able to compare the simulations with experiments, we need to ensure, that the boundary conditions are as close as possible to the real settings of the experiment.

5.4.1 Inlets and outlets

Methane inlet

In the experiment we decided to let the methane stream in the burner at a constant overpressure of 0,5 kPa. Since with compressible fluid it is better to work with mass flow inlets instead of pressure inlets, it was necessary to compute the methane inlet flow rate, as flow meter was not yet available in the preliminary experiment.

The computation of a mass flow rate through a given geometry is not as easy as it seems. The reason is that the flow in the geometry (a small straight cylindrical pipe in our case) is not uniform – the fluid particles near the walls move slower than particles around the cylinder axis and particles adjacent to the wall do not move at all. In literature can be found some formulas for calculating the so called effective diameter of a cylinder flow, but these relations are only approximate. To be as accurate as possible I numerically solved the flow problem and computed the mass flow rate using Fluent.

To compute the mass flow rate, I generated a new geometry and set the boundary conditions as can be seen in Fig 5-2. The turbulence model used was $k-\varepsilon$ realizable with default settings. After the solution converged I used the post-processing tools to compute the methane mass flow rates at different positions in the nozzle. Finally, I averaged all values to get the reference value (see Tab 5-1). The computed value was very close to the measured value (see Tab 4-2)

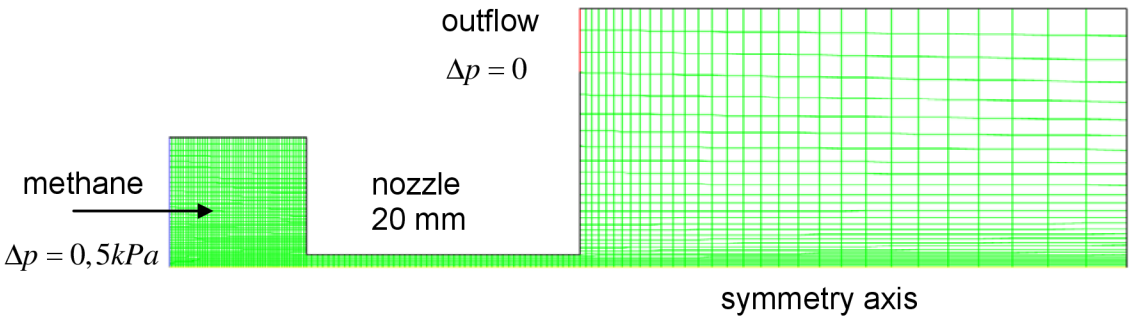

Fig 5-2 *Mesh generated in Gambit*

With the data collected form this simulation I was also able to extract velocity profiles of the flow in the nozzle. I defined a number of surfaces (perpendicular to the axis) and used them to plot the velocity profiles (see Fig 5-3). The figure may seem confusing, as the blue colour is used twice. But it is easy to realize, that the plot x=22 mm is not anymore in the nozzle and therefore there are non-zero velocities beyond 1 mm in radial direction.

In the figure we can notice, that during the first millimetre the velocity profile rapidly changes from its overall minimum to maximum while still having concave shape. Further on downstream the shapes become convex and the peaks of the velocity profiles slowly diminish.

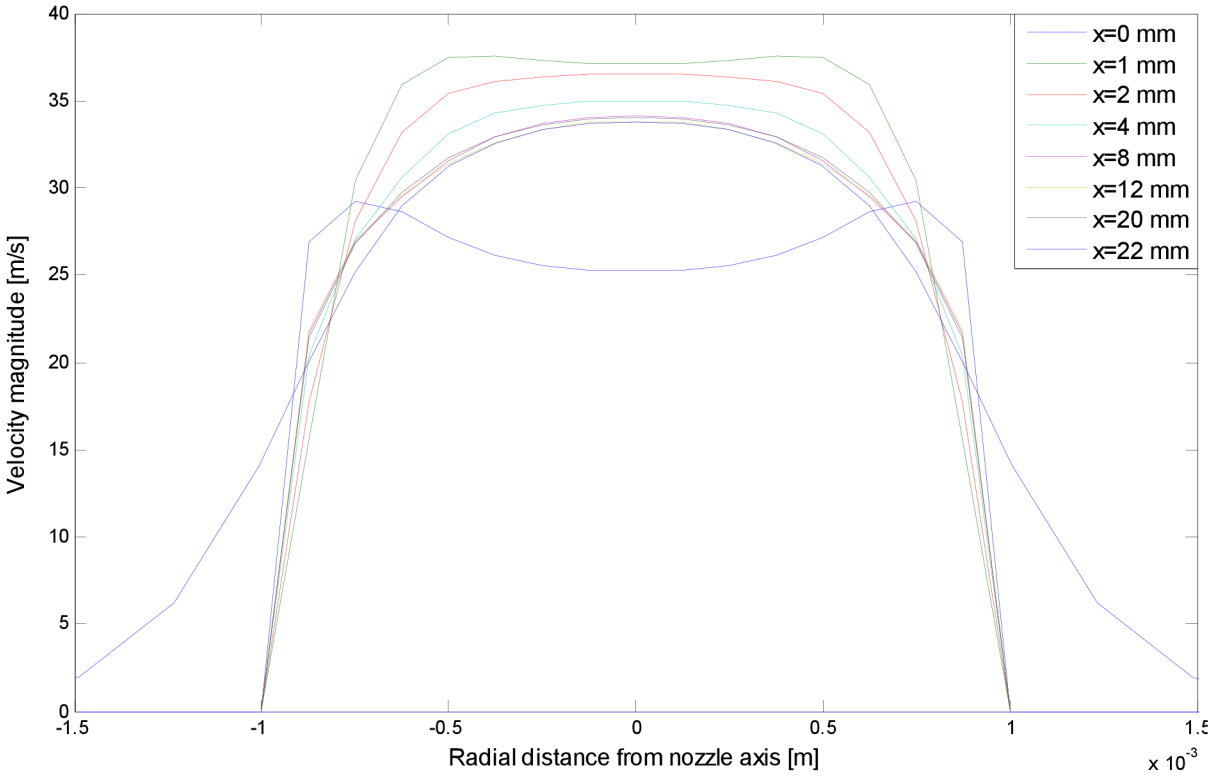

Fig 5-3 *Nozzle velocity profiles in different radial cuts, the nozzle is 20 mm long*

In the experiment the methane gas travels a relatively long distance between the bottle and the nozzle. Thus when the flow reaches the nozzle it can be considered fully turbulent. This distance is of course much greater that the distance traveled by the fluid in the computational mesh. To take into account the fully developed turbulent flow, it is sufficient to set the inlet turbulent properties as written in Tab 5-1 (FLUENT 2005).

Air inlet

Defining the air inlet boundary presented an intriguing challenge. As metnioned before (chapter 3), a reasonable air coflow has stabilizing effects on the flame both in the experiment and simulation, but increased co-flow quickly destabilises the flame. In order to generate a suitable coflow during the experiment we would need a wind tunnel, which was beyond our possibilities. In fact, during the experiment we tried by all means to minimize the air circulation around the burner.

In the near burner region an air draft emerges due to the air entrainment in the fuel stream and subsequent combustion. This entrainment-induced air draft is easily possible to model, but as I found out, without an added coflow the solution exhibits instabilities and may not converge at all. To remedy this issue I tried to add an air stream coming from the top in downward direction (orientation according to Fig 5-1). This approach improved the stability issue but the rate of convergence was not as big as compared to the air coflow approach, while the field predictions were almost identical. Therefore I decided to add an air coflow. The coflow speed was selected as small as possible, in order to not jeopardise the solution stability.

The air inlet boundary type was set to velocity inlet. Generally this setting is inappropriate for compressible fluids (see section 5.3). But in our case, given the very

low air entrance speed, it does not pose any difficulty. The setting details can be seen in Tab 5-1.

Tab 5-1 *Inlet and outlet boundary conditions*

	Methane	Air	Outflow
Type of boundary	Mass flow inlet	Velocity inlet	Pressure outflow
Value	5,593 e-5 kg/s	0,5 m/s	0 Pa
Direction	Normal to boundary	Normal to boundary	Normal to boundary
Turbulent intensity	10%	5%	-
Hydraulic diameter	2 mm	284 mm	-
Backflow turb. intensity	-	-	5%
Backflow turb. length scale	-	-	300 mm
Temperature[1]	20°C	20°C	-
Composition[1]	100% CH_4	23,31% O_2, 76,005% N_2 0,627% H_2O, 0,058% CO_2	-
Mixture fraction[2]	1	0	-
Mixture fraction variance[2]	0	0	-

[1] only applies when one of the following models is used: ED, EDC, LFR or PDF Transport
[2] only applies when one of the following models is used: Equilibrium, Steady laminar flamelet

When the equilibrium and Steady laminar flamelet models are used, the temperature and composition properties of methane and air are input while setting up the models and generating the PDF look-up table.

5.4.2 Axis and Walls

The boundary type of the symmetry axis in Fig 5-1 was set to “axis”. This means, that FLUENT will treat the symmetry axis as a centerline of an axisymmetric geometry (zero normal gradients). No inputs are needed.

All the remaining parts of the boundary are set to “wall” with default settings, in which the heat flux is set to zero (adiabatic).

5.5 Balance calculations

To ensure there is enough air for the combustion process I performed a balance calculation. Using the data in Tab 5-1 and Fig 5-1 I calculated the molar flow rates of methane and oxygen, and with the knowledge of the methane oxidation reaction I was able to compute the so-called *air equivalence ratio* $\phi = 47,27$. This means that there is approximately 47-times more air then theoretically needed for complete oxidation of the fuel.

5.6 Solution strategy

All the simulations were carried out according to the following strategy:

1) Load the mesh file, check and scale the grid
2) Enable the energy equation (the energy equation will be automatically disabled when choosing the adiabatic nonpremixed models)
3) Choose the turbulence and chemistry models and retain the default settings
4) Define material properties and boundary conditions
5) Initialize the solution and start the iteration process
6) Upon convergence, improve the discretization schemes
7) Upon convergence, restrict convergence criteria
8) Upon convergence, declare as a converged solution

In the list above, discretization schemes are mentioned. FLUENT offers various discretization schemes to choose from. The default (and basic) scheme for all involved transport equations is the first order upwind scheme and in the case of pressure equation the so-called standard scheme. In step 6) I usually improved only the following transport equations (if and when used): flow equations (including pressure, momentum and density) and the transport equations for $\overline{f}$ and $\overline{f'^2}$. In these equations I used the second order upwind scheme and in the case of pressure equation the second order scheme. Almost in all cases the second order discretization schemes led only to a small refinement of the solution.

FLUENT stops the iteration process when all residuals fall below a predefined criterion. The default choice for all residuals is 10^{-3} and in the case of energy equation 10^{-6}. When restricting the convergence criteria as stated in 7), I repeatedly decreased the criterion of the slowest converging equation until all residuals levelled out.

5.7 Results

This section provides a summary of computed results and comparison of the various models employed.

5.7.1 Cold run

In this simulation the goal was to compare different turbulence models (namely $k-\varepsilon$ standard, $k-\varepsilon$ RNG, $k-\varepsilon$ realizable, $k-\omega$ standard and RSM model) focusing on the mass fraction of methane in dependence to the axial distance from the nozzle without considering the chemistry interactions, or in other words – pure methane-air mixing.

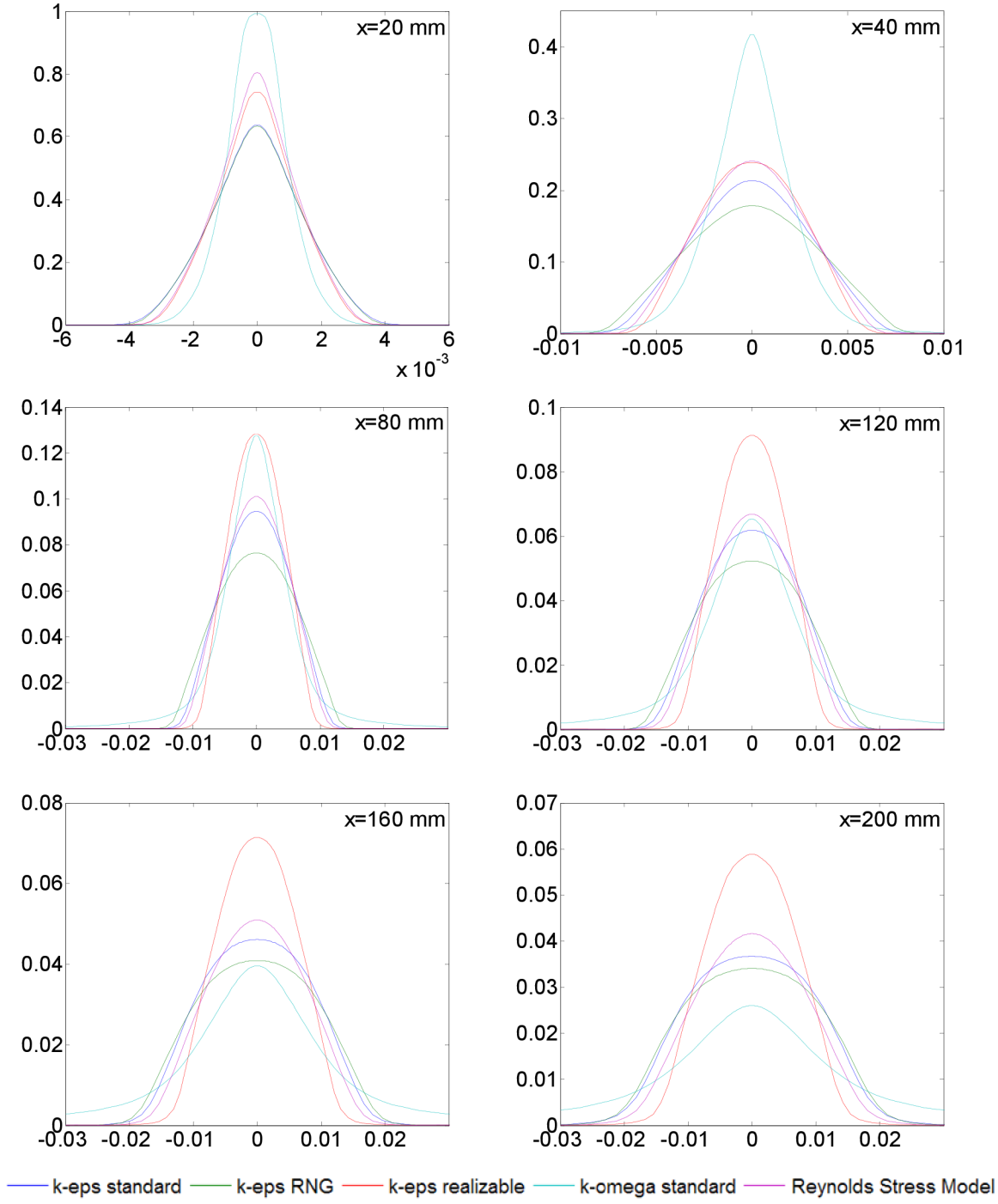

Fig 5-4 *The vertical axis represents the mixture fraction while the horizontal axis represents radial distance form the axis in [m]. The quantity x represents the distance from the methane inlet.*

Plots in Fig 5-4 and Fig 5-5 show the methane mass fraction radial profiles at different axial distance. It is apparent, that the superior RSM turbulence model gives very similar predictions to the $k-\varepsilon$ models. The most outlaying predictions are given by the $k-\omega$ standard model.

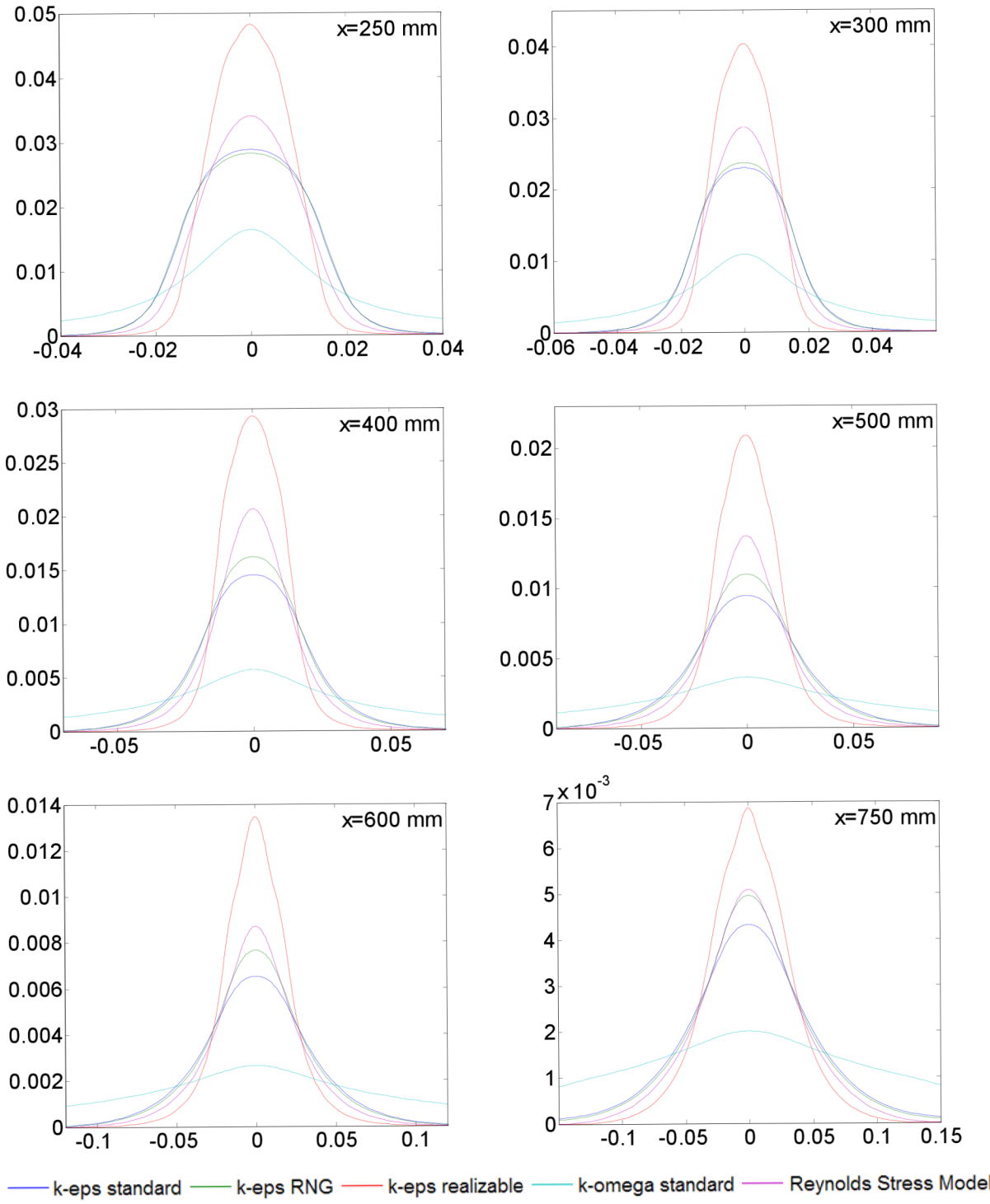

Fig 5-5 *The vertical axis represents the mixture fraction while the horizontal axis represents radial distance form the axis in [m]. The quantity x represents the distance from the methane inlet.*

5.7.2 Combustion simulations

In all the simulations including chemistry interaction discussed from now on the $k-\varepsilon$ realizable turbulence model will be used. I chose this model, because it should give accurate predictions of round (and planar) jet spreading rate (FLUENT 2005). The converged "cold flow" solution of this model is used as initial data for simulations discussed in this part.

ED model

In the simulations, three different ED model settings were used – ED model with one-step, two-step global reaction mechanism and one-step global reaction mechanism with constant c_p. The temperature predictions can be found in Fig 5-8a and Fig 5-6.

In Fig 5-8a can be seen, that the two-step global reaction mechanism gives almost identical temperature prediction throughout the computational domain. The model with constant c_p on the other hand over predicts temperatures in the whole combustion region (see Fig 5-6).

Equilibrium model

The equilibrium model provides a small improvement over the previous model within the meaning of maximum temperature prediction. However it under-predicts temperatures in the first approximately 250 mm long region. From Fig 5-6 and Fig 5-8b can be seen, that this under prediction occurs only near to the axis.

Steady laminar flamelet model

In the Steady laminar flamelet model four different reaction mechanisms were used for generating the PDF look-up tables – Reduced, Smooke, Kee and Gri-MECH 3.0 mechanism. Every one of them outperformed both previously mentioned models in terms of temperature and OH radical prediction (see Fig 6-2).

When compared with each other only small temperature differences were observed. In Fig 5-7 and Fig 5-8c can be seen that all plots are very much alike. Only the Gri-MECH mechanism can present an exception, when in the last two plots slightly over-predicts the temperatures with respect to the other mechanisms.

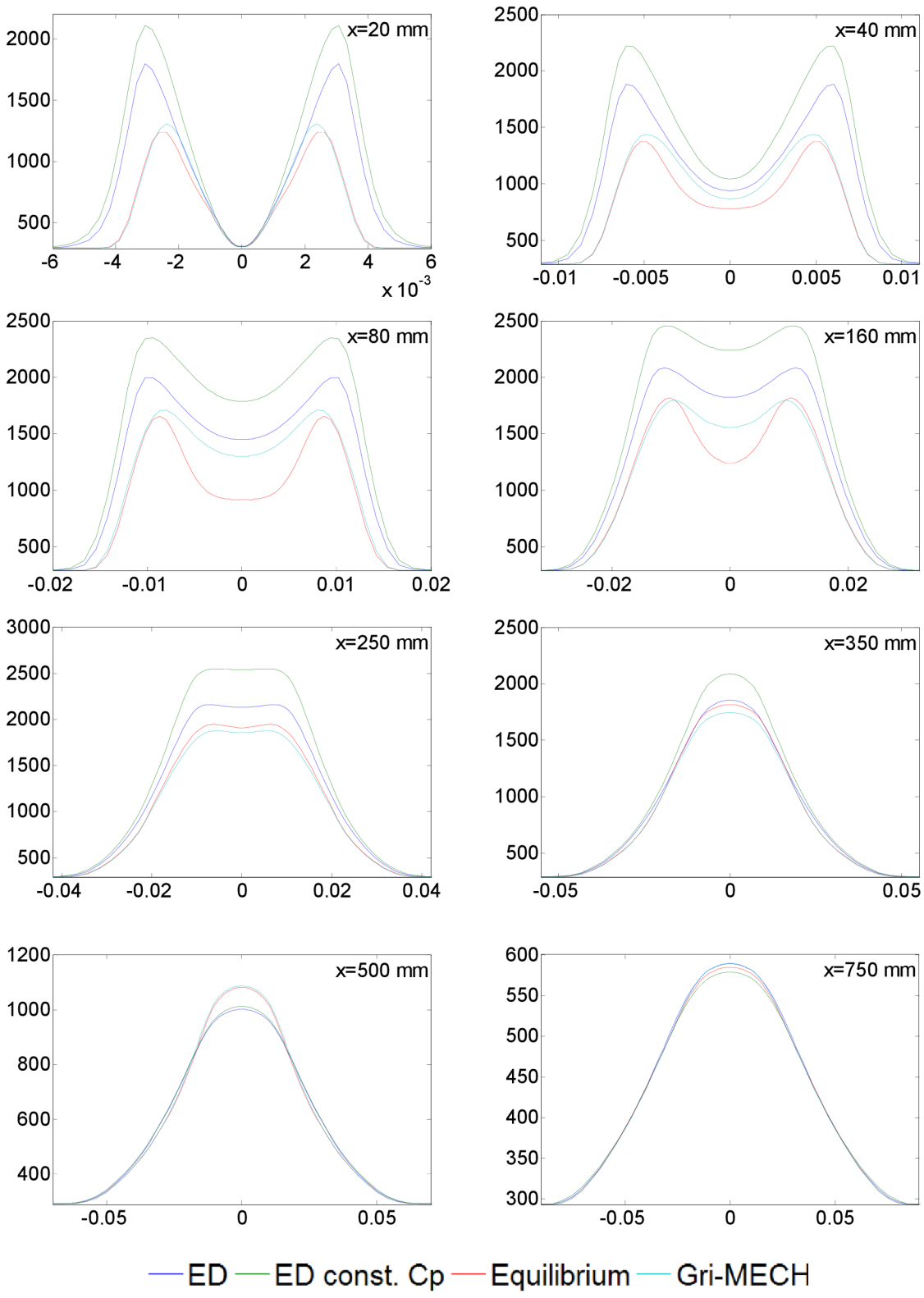

Fig 5-6 *Vertical axis represents the temperature in [K] while the horizontal axis represents radial distance form the axis in [m]. The quantity x represents the distance from the methane inlet. Gri-MECH corresponds to the Steady laminar flamelet model with the Gri-MECH mechanism*

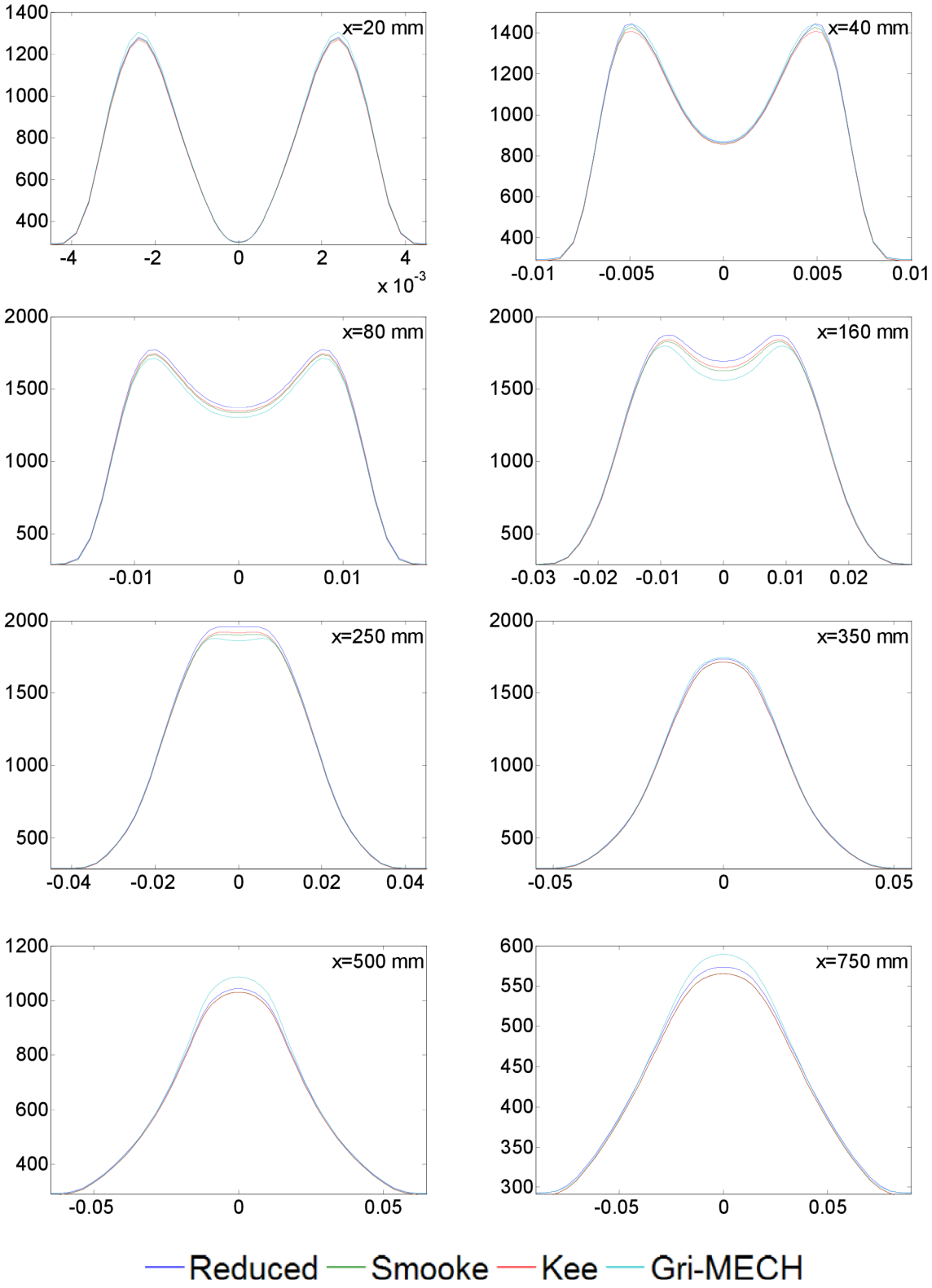

Fig 5-7 *Vertical axis represents the temperature in [K] while the horizontal axis represents radial distance form the axis in [m]. The quantity x represents the distance from the methane inlet. Gri-MECH, Kee, Smooke and Reduced correspond to the Steady laminar flamelet model with the matching mechanism*

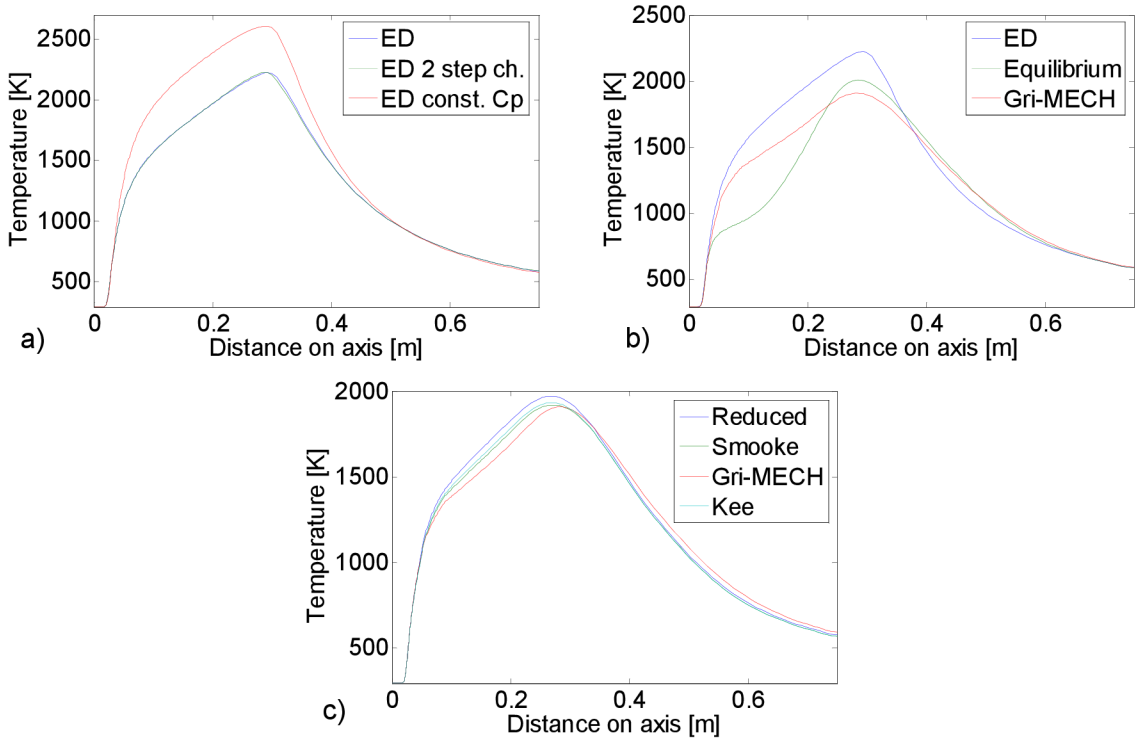

Fig 5-8 *Axial temperature,; Gri-MECH, Kee, Smooke and Reduced correspond to the Steady laminar flamelet model with the matching mechanism*

EDC, PDF, LFR

Models used so far were unable to predict more complex flame phenomena like flame lift-off. This is due to the fact that they all more or less use the assumption of slow mixing and fast burning. In the experiment we chose a specific setup that enables the flame to exhibit both the attached and lifted regime. To model the lift-off phenomenon I was obliged to use more complex models, namely EDC model and PDF-transport model. As mentioned in section 5.1.2, these models can also benefit from detailed reaction mechanisms. To provide information about the species and reactions, the same mechanisms as in the previous section were used.

Unfortunately, at this point I started encountering difficulties. Both EDC and PDF models behaved in a similar manner: the simulation was started using the converged solution from the steady laminar flamelet model, but during the first tens solution iterations, the flame was blown off for no apparent reason. Neither subsequent forced ignition nor decrease of the methane inlet mass flow rate nor change in the air co-flow speed helped to stabilize the lifted flame.

The same behaviour (blowoff) was observed (and documented in video files) also after including time into the formulation and performing an unsteady simulation with initial condition defined by a converged laminar flamelet solution with the same chemical mechanism. In order to stabilise the flame under these circumstances,

artificial flame holder would probably be necessary, e.g. an artificial hot spot on the burner rim.

It is hard to establish the precise reason for the instability using these advanced models, but the instability phenomenon has been observed also in the experiment, although the detailed behaviour was different. So it can be that the used computational setup in some unidentified way makes the region of stability even more limited than in practice. Various parameters including inlet turbulence intensity or two-dimensionality of the model may influence the observed behaviour. Further investigations would be necessary to determine the precise cause.

6 Discussion

One of the goals of this thesis was to compare different turbulence models. As mentioned in section 5.7.1 a simulation was carried out to compare the "mixing skills" of each model. When analyzing plots in Fig 5-4 and Fig 5-5 the first thing worth mentioning is that the $k-\varepsilon$ standard and the $k-\varepsilon$ RNG model give very similar predictions. This is because in our particular case, the flow is not rapidly strained or swirling and therefore the superiority of the $k-\varepsilon$ RNG model could not fully manifest itself.

The $k-\varepsilon$ realizable model gives very similar predictions to the RSM close to the nozzle orifice (up to 40 mm downstream). Further on it starts to over-predict axial methane mixture fractions with respect to all other tested models. As far as the spreading in radial direction is concerned, the $k-\varepsilon$ realizable model gives the lowest mixture fraction predictions.

As for the $k-\omega$ standard model, its predictions differ from all other turbulence models taken into account. The $k-\omega$ model over predicts the methane mixture fraction on the axis up to the first 40 mm but also predicts small amounts of methane in the peripheral regions (in radial direction) from the very end of the nozzle. In other words, the methane stream does not spread much in this region, but the bit that does is quickly spread in radial direction. In the region between 80 and 160 mm the axial methane mixture fractions are similar to the other turbulence models but the $k-\omega$ model predictions start to differ again when we get beyond 200 mm downstream from the nozzle. In this region the axial mixture fractions are greatly under predicted while the radial spreading is over predicted.

Perhaps surprisingly, the $k-\varepsilon$ models give very similar predictions to the RSM model throughout the whole domain. This is caused mainly due to the relative flow simplicity. The RSM model proves his superiority only in more complex flows, like cyclone flows, highly swirling flows in combustors, rotating flow passages, and the stress-induced secondary flows in ducts, none of which is our case.

The main goal of this thesis lies in simulating a jet diffusion flame. I carried out numerous simulations using different chemical models and reaction mechanisms. The basic model for such simulations is the Eddy-Dissipation model. Three variations of this model were used and compared (see Fig 5-8a and Fig 5-6).

It turned out that in my specific case there was almost no difference between the temperature predictions when comparing one- and two-step reaction mechanism, except for the fact that the two-step mechanism was logically computationally more expensive. An example of this similarity can be found in Fig 5-8a. On the other hand, the ED model with constant c_p hugely over predicted temperatures throughout the combustion region (see Fig 5-8a and Fig 5-6). As mentioned in section 5.3, choosing this coefficient to be constant is not a good choice when modelling combustion, because the constant-pressure specific heat depends strongly on temperature.

The next logical step in the sense of performance was the equilibrium model. From Fig 5-6 and Fig 5-8b we can see that this model predicts smaller temperatures than the eddy-dissipation model, which is definitely a sign of improvement.

Another significant improvement is achieved when employing the steady laminar flamelet model thank to the more detailed reaction mechanisms it allows us to use. When comparing the different mechanisms among themselves in terms of temperature predictions (see Fig 5-7), we can see that none of them diverges from the others in a noticeable way. A more notable (but still not significant) difference between the mechanisms can be seen in Fig 6-2. In this contour, where the OH mass fraction is portrayed, we can see that both Kee and Smooke mechanisms slightly over predict the presumably accurate Gri-MECH mechanism. Surprisingly the Reduced mechanism (least detailed mechanism considered) gets ahead of Kee and Smooke mechanisms in this case.

These similarities suggest that the considered reacting flow problem was not complex enough for the mechanisms differences to manifest. The Gri-MECH reaction mechanism is considered to be the most detailed reaction mechanism for methane combustion so far created. Newly proposed mechanisms are usually compared with it. This is the reason why in other comparison plots the Reduced, Smooke and Kee mechanisms are ignored.

Stronger differences are observed when comparing the steady laminar flamelet model (with Gri-MECH 3.0 mechanism) with the two previously mentioned models. In Fig 5-8b we can see, that the steady laminar flamelet model predictions have a very similar shape to the eddy-dissipation model predictions. Still, in the region up to approximately 400 mm downstream from the nozzle ED over predicts the temperature while in the remaining region ED under predicts the temperature (see Fig 5-8b and Fig 5-6). When the steady laminar flamelet model is compared with the equilibrium model, only small discrepancies appear. The most notable one is in the axial temperatures prediction (see Fig 5-8b). In the region up to approximately 250 mm the equilibrium model under-predicts the temperature. This temperature under prediction is probably caused by the “strong” chemical equilibrium assumption. It looks like the equilibrium assumption “slows” the air entrainment towards the axis and thus the oxygen burns before it can get to the “cold” region. This changes further downstream, where the methane stream is less compact and easily mixes with air. The steady laminar flamelet model improves the temperature prediction in this area because it accounts for (moderate) non-equilibrium states. Apart from the discrepancies in temperature predictions among the steady laminar flamelet, equilibrium and eddy-dissipation models, the overall shape of the temperature contour remains very similar for all models (see Fig 6-3).

Another notable difference can be seen in Fig 6-2 where the equilibrium model clearly over predicts the OH mass fraction. This is again probably caused by the chemical equilibrium assumption. On the other hand, regardless of the mass fraction over-prediction, the length and shape of the contour calculated by the equilibrium model is closest to the Gri-MECH prediction among all other mechanisms.

As mentioned in section 5.7.2, I encountered sudden flame blowoff while using the EDC and PDF Transport models. When trying to get at the bottom of this stability issue various approaches were tested to eliminate the problem that could be hidden e.g. in the three dimensional nature of the problem as mentioned above. If the flame would be allowed to flutter, the axis boundary condition would impose an axisymmetric swelling, which could cause high strain rates leading to flame

extinction. To remedy this shortcoming a three dimensional simulation was performed, but the solution behaved in the exact same manner as before.

The last, but for sure not the least important goal, was to follow through an experiment and compare the predicted results. The preliminary experiment took place in February 2009 while the spectrometric experiment took place in April 2009. During this period I was performing all simulations based on the decisions made in the preliminary experiment. Of course nobody at that time could have known that we will be unable to reproduce the desired flames at the other laboratory. In order to provide means for validation I performed a last-minute simulation with altered boundary conditions (methane mass flow rate at inlet was set as in #1 in Tab 4-2) in order to ensure the comparability of the prediction with the experiment. In this simulation I used the steady laminar flamelet model with Gri-MECH 3.0 reaction mechanism along with the $k-\varepsilon$ realizable model (as the best of the compared alternatives). Due to the problems with EDC and PDF Transport model I could only simulate the attached flame regime and could therefore compare the predicted results only with configuration #1 in Tab 4-2.

In Fig 6-1 we can see the comparison of axial temperatures between the model predictions and two experimental calculations. The plot suggests that the rotational temperatures computed using the CH rotational spectrum reflects better the actual flame temperatures than the OH rotational temperatures. We could therefore say that the used model shows good agreement with the experiment. However, we have to keep in mind that the conditions during the spectrometry measurement were far from ideal.

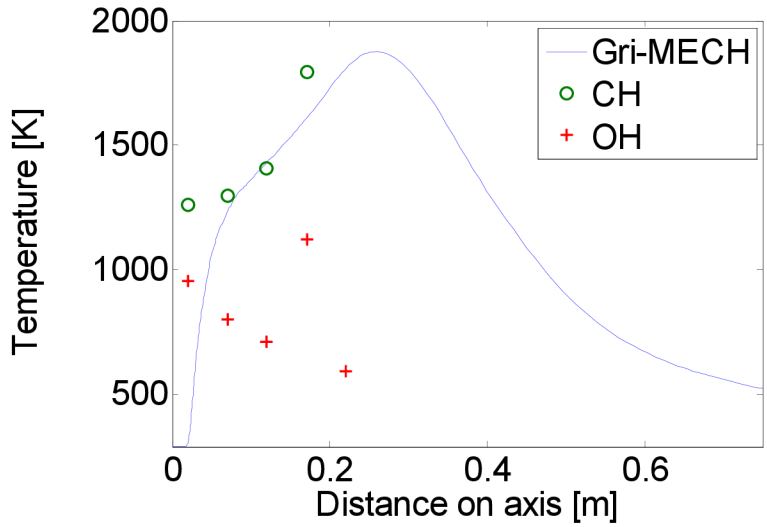

Fig 6-1 *Comparison between simulation and experiment*

To sum up the relevant results, when modelling a relatively simple combustion problem, without complex flow characteristics, the best halfway decision between accuracy and computational time is the steady laminar flamelet model with a reduced chemical mechanism combined with the $k-\varepsilon$ realizable turbulence model. The $k-\varepsilon$ realizable model gives no worse predictions than the RSM model, while saving computational time and the steady laminar flamelet model accounts for slight non-equilibrium effects, which are part of almost all practical combustion applications, and

can predict intermediate and radical species. Thanks to the pre-processed PDF look-up tables it provides tremendous savings in terms of computational time, while delivering relatively accurate predictions. Its only shortcoming is the impossibility to account for stability issues like, flame lift-off and extinction.

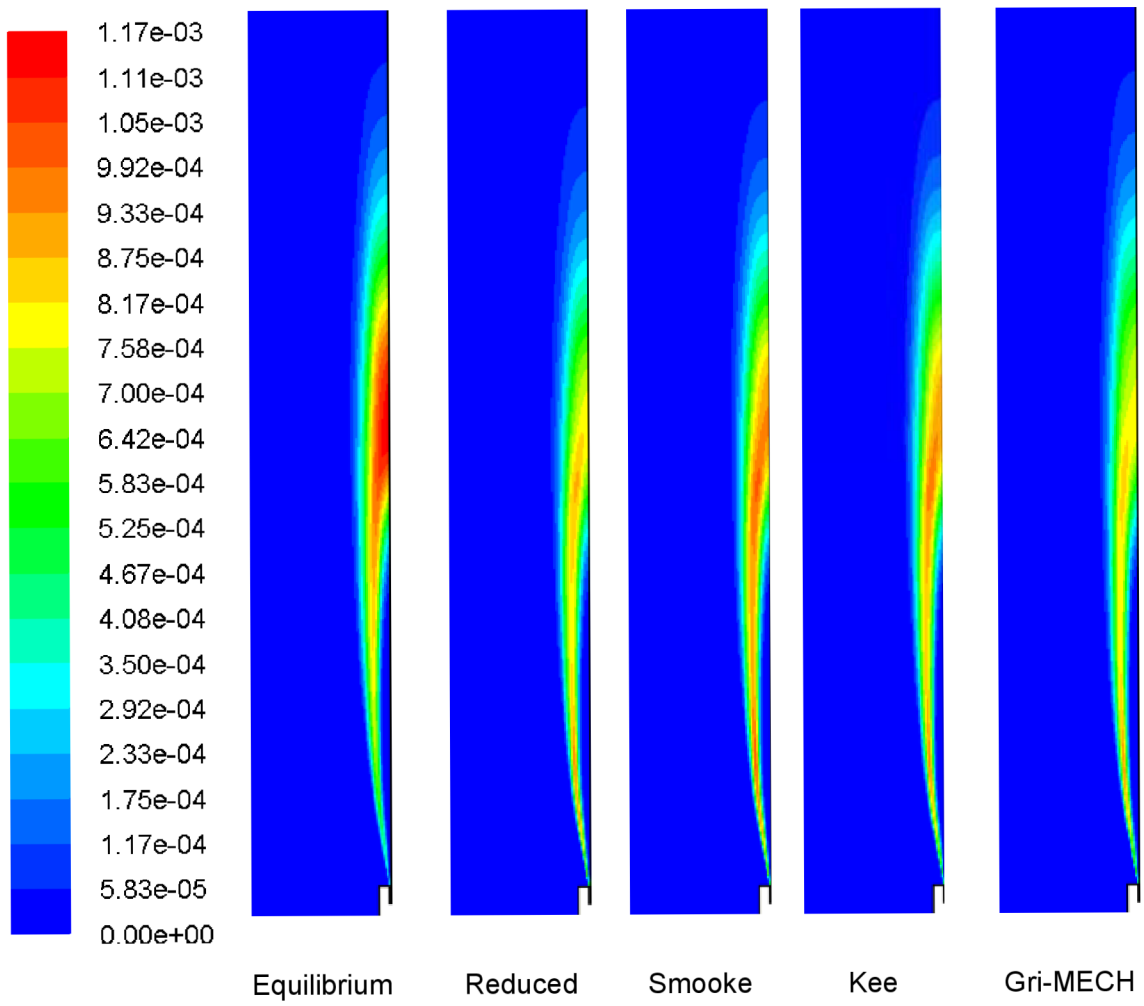

Fig 6-2 *Mass fractions of OH radical, Gri-MECH, Kee, Smooke and Reduced correspond to the Steady laminar flamelet model with the matching mechanism*

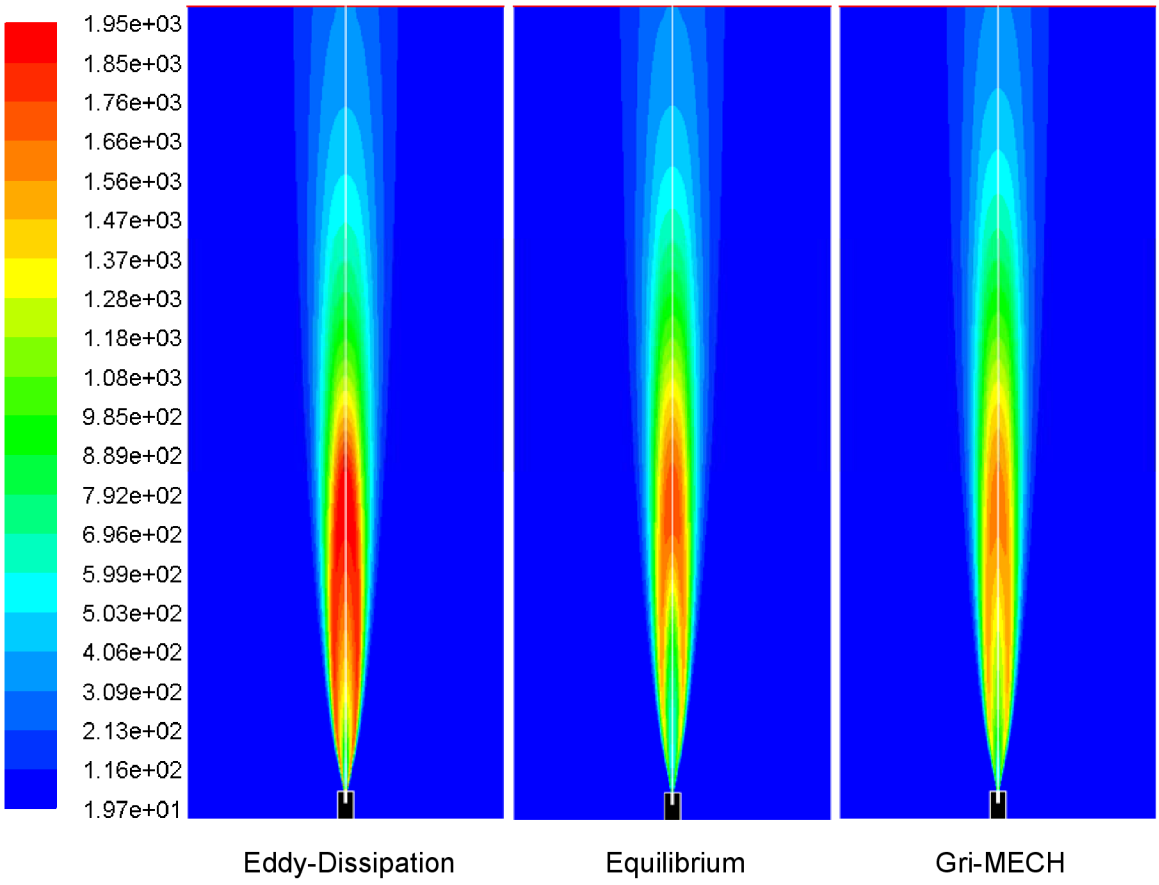

Fig 6-3 *Temperature contours [°C], Gri-MECH, Kee, Smooke and Reduced correspond to the Steady laminar flamelet model with the matching mechanism*

7 Conclusion

The aim of this thesis was to follow through a simulation of a simple combustion problem, compare different combustion models and finally confront the predicted results with experimental data. In the first part of the thesis I provided a theoretical introduction into this field. I summarised the most common turbulence and chemistry models and presented a review of recent research in the area investigated in this work. In the following parts both the experiment and simulations were described in detail and obtained results were presented. In the last part I compared all the results and tried to deduce conclusions. It has been shown that even a relatively simple flow problem of a free jet flame may entail serious problems when trying to use complex models. However, I was unable neither to eliminate the predicted instability followed by blowoff in the EDC, PDF and LFR models nor to provide a conclusive explanation of this behaviour. Further research in this area is therefore necessary. It has been however shown that the attached flame regime is reasonably well predicted by models composed of the $k-\varepsilon$ realizable turbulence model and steady laminar flamelet chemistry.

8 References

Chao, Y. et al. Effects of dilution on blowout limits of turbulent jet flames. *Combustion Science and Technology*, 2004, 176(10), 1735-1753.

Chen, M., Herrmann, M. & Peters, N. Flamelet modeling of lifted turbulent methane/air and propane/air jet diffusion flames. *Symposium (International) on Combustion*, 2000, 28(1), 167-174.

Domingo, P., Vervisch, L. & Bray, K. *Combust. Theory Modeling*, 2002, 6, 529–551.

Fairweather, M. & Woolley, R.M. First-order conditional moment closure modeling of turbulent, nonpremixed methane flames. *Combustion and Flame*, 2004, 138(1-2), 3-19.

Fallot, L. et al. Modeling finite-rate chemistry effects in nonpremixed turbulent combustion: Test on the bluff-body stabilized flame. *Combustion and Flame*, 1997, 110, 298-314.

Ferraris, S. & Wen, J. Large eddy simulation of a lifted turbulent jet flame. *Combustion and Flame*, 2007, 150(4), 320-339.

FLUENT 6.3 User's Guide, Fluent, Inc., Lebanon, 2005

Hájek, J. *Modelování s využítím CFD – I.* Electronic study material (in Czech), 2007.

Hamins, A. et al. Effect of buoyancy on the radiative extinction limit of low-strain-rate nonpremixed methane-air flames. *Combustion and Flame*, 2007, 151, 225-234.

Jones, W.P. & Kakhi, M. Pdf Modeling of Finite-rate Chemistry Effects in Turbulent Nonpremixed Jet Flames. *Combustion and Flame*, 1998, 115(1-2), 210-229.

Kiran, D. & Mishra, D. Experimental studies of flame stability and emission characteristics of simple LPG jet diffusion flame. *Fuel*, 2007, 86(10-11), 1545-1551.

Lawn, C.J. Lifted flames on fuel jets in co-flowing air. *Progress in Energy and Combustion Science*, 2009, 35(1), 1-30.

Leung, T. & Wierzba, I. The effect of co-flow stream velocity on turbulent non-premixed jet flame stability. *Proceedings of the Combustion Institute*, 2009, 32(2), 1671-1678.

Lock, A. et al. Liftoff and extinction characteristics of fuel- and air-stream-diluted methane-air flames. *Combustion and Flame*, 2007, 149(4), 340-352.

Mahalingam, S., Chen, J.H & Vervisch, L. Finite-rate chemistry and transient effects in direct numerical simulations of turbulent nonpremixed flames. *Combustion and Flame*, 1995, 102, 285-290.

Mahmud, T. et al. Experimental and computational study of a lifted, non-premixed turbulent free jet flame. *Fuel*, 2007, 86(5-6), 793-806.

Muniz, L. & Mungal, M.G. Instantaneous flame-stabilization velocities in lifted-jet diffusion flames. *Combustion and Flame*, 1997, 111(1-2), 16-30.

Norris, A.T. & Pope, S.B. Modeling of extinction in turbulent diffusion flames by the velocity-dissipation-composition PDF method. *Combustion and Flame*, 1995, 100(1-2), 211-220.

Otakeyama, Y., Yokomori, T. & Mizomoto, M. Stability of CH4-N2/air jet diffusion flame for various burner rim thicknesses. *Proceedings of the Combustion Institute*, 2009, 32(1), 1091-1097.

Peeters, T. *Numerical Modeling of Turbulence Natural-Gas Diffusion Flames*. PhD thesis, Delft Technical University, Delft, The Netherlands, 1995.

Raman, V., Pitsch, H. & Fox, R.O. Hybrid large-eddy simulation/Lagrangian filtered-density-function approach for simulating turbulent combustion. *Combustion and Flame*, 2005, 143, 56-78.

Sanders, J.P.H., Sarh, B. & Gökalp, I. Variable density effects in axisymmetric isothermal turbulent jets: a comparison between a first- and a second-order turbulence model. *International Journal of Heat and Mass Transfer*, 1997, 40(4), 823-842.

Shaw, C.T. *Using Computational Fluid Dynamics*, Prentice Hall, 1992, [online], [cit 2009-5-10], URL: <http://www.topajka-shaw.com.nz/UFEND.html>

Smith, G.P., Golden, D.M., Frenklach, M., Moriarty, N.W., Eiteneer, B., Goldenberg, M., Bowman, C.T., Hanson, R.K., Song, S., Gardiner Jr., W.C., Lissianski, V.V. & Qin, Z., [online], [cit 2009-5-26], URL: < http://www.me.berkeley.edu/gri_mech/>

Smooke, M.D., Puri, I.K. & Seshadri, K. A comparison Between Numerical Calculations and Experimental Measurements of the Structure of a Counterflow Diffusion Flame Burning Diluted Methane in Diluted Air. *21st Symp. on Combustion*, The Combustion Institute. 1986, 1783-1792.

Smooke, M.D. Reduced Kinetic Mechanisms and Asymptotic Approximations for Methane-Air Flames. *Lecture Notes in Physics*, volume 384, Springer-Verlag, 1991.

Taing, S. & Masri, A. R. PDF Calculations of Turbulent Nonpremixed Flames of H_2/CO_2 Using Reduced Chemical Mechanisms. *Combustion and Flame*,1993, 95, 133-150.

Torii, S., Jung, B. & Yano, T. Reignition phenomenon of high-speed hydrogen jet diffusion flame. *International Journal of Energy Research*, 2002, 26(12), 1045-1053.

Warnatz, J., Maas, U. & Dibble, R.W. *Combustion*, Springer-Verlag Berlin Heidberg, 2001.

Wu, C. et al. The blowout mechanism of turbulent jet diffusion flames. *Combustion and Flame*, 2006, 145(3), 481-494.

9 Nomenclature and acronyms

c_v	[J.kg-1.K^{-1}]	constant-volume specific heat
$C_{1\varepsilon}, C_{2\varepsilon}, C_{3\varepsilon}, C_\mu$	[-]	model constants
C_ξ	[-]	volume fraction constant
C_τ	[-]	time scale constant
$D_{i,m}$	[m^2.s^{-1}]	diffusion coefficient for species *i* in the mixture
D_t	[m^2.s^{-1}]	turbulent diffusivity
e	[J.kg^{-1}]	specific energy
E_r	[J]	activation energy for the reaction r
f	[-]	mixture fraction
$\mathbf{f}$	[N]	volume forces
G_b	[kg.m^{-1}.s^{-3}]	generation of turbulence kinetic energy due to buoyancy
G_k	[kg.m^{-1}.s^{-3}]	generation of turbulence kinetic energy due to the mean velocity gradients
G_ω	[kg.m^{-3}.s^{-2}]	generation of ω
H	[J]	enthalpy
$\mathbf{J}_i$	[kg.m^{-2}.s^{-1}]	diffusion flux of species i, which arises due to concentration gradients.
k	[m^2.s^{-2}]	turbulent kinetic energy
k	[W.m^{-1}.K^{-1}]	thermal conductivity
$k_{f,r}, k_{b,r}$	[mol^{1-n}. m^{3n-3}.s^{-1}]	forward, respectively backward constant rates for reaction r of order n
K_r	[-]	equilibrium constant for the reaction r
$M_{w,i}$	[kg.mol^{-1}]	molecular mass of species *i*
M_S	[kg.mol^{-1}]	molar mass
p	[Pa]	pressure
R	[J.mol^{-1}.K^{-1}]	universal gas constant

$R_{i,r}$	[kg.m^{-3}.s^{-1}]	rate of creation of species *i* due to reaction *r*
$\hat{R}_{i,r}$	[kg.m^{-3}.s^{-1}]	Arrhenius molar rate of creation/destruction of species i in reaction r
S_i	[kg.m^{-3}.s^{-1}]	rate of creation by addition
S_k	[kg.m^{-1}.s^{-3}]	user-defined source term
S_ε	[kg.m^{-1}.s^{-4}]	user-defined source term
S_ω	[kg.m^{-3}.s^{-2}]	user-defined source term
T	[K]	temperature
$\mathbf{v}$	[m.s^{-1}]	velocity
Y_i , w_i	[-]	mass fraction of species *i*
Y_k	[kg.m^{-1}.s^{-3}]	dissipation of k due to turbulence
Y_ω	[kg.m^{-3}.s^{-2}]	dissipation of ω due to turbulence
Y_M	[kg.m^{-1}.s^{-3}]	contribution of the fluctuating dilatation in compressible turbulence to the overall dissipation rate
Y_{R}	[-]	mass fraction of a particular reactant R
Y_{P}	[-]	mass fraction of any product species P
Z_i	[-]	elemental mass fraction for element i
α^*	[-]	turbulent viscosity damping coefficient
β_r	[-]	temperature exponent
χ	[kg.m^{-4}]	scalar dissipation
ε	[m^2.s^{-3}]	turbulent dissipation
ϕ	[-]	Air equivalence ratio
φ,ψ	[-]	arbitrary functions
λ	[kg.m^{-1}.s^{-1}]	second viscosity coefficient
μ	[kg.m^{-1}.s^{-1}]	dynamic viscosity
μ_t	[kg.m^{-1}.s^{-1}]	turbulent viscosity

ν	[$m^2.s^{-1}$]	kinematic viscosity
ω	[s^{-1}]	specific turbulent dissipation
ν_t	[$m^2.s^{-1}$]	turbulent exchange coefficient
ρ	[$kg.m^{-3}$]	density
$\sigma_k, \sigma_\varepsilon, \sigma_\omega$	[-]	turbulent Prandtl numbers for k, ε and ω, respectively
$\tau_{i,j}$	[$J.m^{-3}$]	stress in the plane perpendicular to axis i in the direction j
$\upsilon'_{i,r}$	[-]	stochiometric coefficient for reactant i in reaction r
$\upsilon''_{i,r}$	[-]	stochiometric coefficient for product i in reaction r

CFD	Computational Fluid Dynamics
DNS	Direct Numerical Simulation
DTRM	Discrete Transfer Model
ED	Eddy-Dissipation
EDC	Eddy-Dissipation Concept
FVM	Finite Volume Method
LES	Large-Eddy Simulation
LMSE	Linear Mean Square Estimate
MCM	Moment Closure Methods
OTFRM	Optically Thin Flame Radiation Model
PDF	Probability Density Function
RANS	Reynolds-averaged Navier-Stokes
SGS	Sub-Grid Scale